Neurobiology of Disease

Peripheral Auditory Nerve Impairment in a Mouse Model of Syndromic Autism

Nathan McChesney,[1*] Jeremy L. Barth,[2*] Jeffrey A. Rumschlag,[4*] Junying Tan,[1] Adam J. Harrington,[3] Kenyaria V. Noble,[1] Carolyn M. McClaskey,[4] Phillip Elvis,[1] Silvia G. Vaena,[5] Martin J. Romeo,[5] Kelly C. Harris,[4] Christopher W. Cowan,[3] and Hainan Lang[1]

[1]Department of Pathology and Laboratory Medicine, Medical University of South Carolina, Charleston, South Carolina 29425, [2]Department of Regenerative Medicine and Cell Biology, Medical University of South Carolina, Charleston, South Carolina 29425, [3]Department of Neuroscience, Medical University of South Carolina, Charleston, South Carolina 29425, [4]Department of Otolaryngology & Head and Neck Surgery, Medical University of South Carolina, Charleston, South Carolina 29425, and [5]Hollings Cancer Institute, Medical University of South Carolina, Charleston, South Carolina 29425

Dysfunction of the peripheral auditory nerve (AN) contributes to dynamic changes throughout the central auditory system, resulting in abnormal auditory processing, including hypersensitivity. Altered sound sensitivity is frequently observed in autism spectrum disorder (ASD), suggesting that AN deficits and changes in auditory information processing may contribute to ASD-associated symptoms, including social communication deficits and hyperacusis. The MEF2C transcription factor is associated with risk for several neurodevelopmental disorders, and mutations or deletions of *MEF2C* produce a haploinsufficiency syndrome characterized by ASD, language, and cognitive deficits. A mouse model of this syndromic ASD (*Mef2c*-Het) recapitulates many of the *MEF2C* haploinsufficiency syndrome-linked behaviors, including communication deficits. We show here that *Mef2c*-Het mice of both sexes exhibit functional impairment of the peripheral AN and a modest reduction in hearing sensitivity. We find that MEF2C is expressed during development in multiple AN and cochlear cell types; and in *Mef2c*-Het mice, we observe multiple cellular and molecular alterations associated with the AN, including abnormal myelination, neuronal degeneration, neuronal mitochondria dysfunction, and increased macrophage activation and cochlear inflammation. These results reveal the importance of MEF2C function in inner ear development and function and the engagement of immune cells and other non-neuronal cells, which suggests that microglia/macrophages and other non-neuronal cells might contribute, directly or indirectly, to AN dysfunction and ASD-related phenotypes. Finally, our study establishes a comprehensive approach for characterizing AN function at the physiological, cellular, and molecular levels in mice, which can be applied to animal models with a wide range of human auditory processing impairments.

Key words: auditory nerve; autism spectrum disorder; glial cell; hearing; macrophages; MEF2C

Significance Statement

This is the first report of peripheral auditory nerve (AN) impairment in a mouse model of human *MEF2C* haploinsufficiency syndrome that has well-characterized ASD-related behaviors, including communication deficits, hyperactivity, repetitive behavior, and social deficits. We identify multiple underlying cellular, subcellular, and molecular abnormalities that may contribute to peripheral AN impairment. Our findings also highlight the important roles of immune cells (e.g., cochlear macrophages) and other non-neuronal elements (e.g., glial cells and cells in the stria vascularis) in auditory impairment in ASD. The methodological significance of the study is the establishment of a comprehensive approach for evaluating peripheral AN function and impact of peripheral AN deficits with minimal hearing loss.

Received Feb. 3, 2022; revised July 27, 2022; accepted Aug. 13, 2022.

Author contributions: H.L. and C.W.C. designed the research; N.M., J.L.B., A.J.H., J.T., K.V.N., C.M.M., J.A.R., S.G.V., M.J.R., A.J.H., K.C.H. and H.L. performed the research; J.A.R., J.L.B., N.M., P.E., K.C.H. and H.L. analyzed data; J.L.B., and H.L. drafted the paper, C.W.C., K.C.H., J.L.B., and H.L. revised the paper, and all authors approved the paper.

This work was supported by National Institutes of Health Grants K18DC018517 to H.L., R01DC012058 to H.L., P50DC000422 to H.L. and K.C.H., Simons Foundation Autism Research Initiative Pilot Award 649452 to H.L. and C.W.C., R01 MH111464 to C.W.C., T32014435 to C.M.M., P30GM103342 to J.L.B., and P20GM103499 to J.L.B. Confocal image collection and analysis were done through Medical University of South Carolina (MUSC) Image facilities that were supported in part by the Cell & Molecular Imaging Shared Resource, MUSC Cancer Center Support P30 CA138313, the SC COBRE Grants P20 GM103542 and P20 GM130457, the MUSC Core Center P30 DK123704, and Shared Instrumentation Grants S10 OD018113 and S10 OD028663. Bioinformatic analysis of RNA-seq data was done through the MUSC Proteogenomics Facility that is supported by NIGMS GM103499 and the MUSC Office of the Vice President for Research. We thank John Lemasters for suggestions with the use of the mitochondrial functional markers; Nancy Smythe, Catherine Bridges, Cindy Wang, Gang Li, Shelby Storm, Juhong Zhu, Carlene Brandon, Jiaying Wu, and Logan Martin for excellent technical assistance; Richard Schmiedt for help with the system setup of single-trial ABR recording; and Jayne Ahlstrom, Nathaniel Parsons, and Cindy Wang for comments and editing of the manuscript.

*N.M., J.L.B. and J.A.R. contributed equally to this work.

The authors declare no competing financial interests.

Correspondence should be addressed to Hainan Lang at langh@musc.edu.

https://doi.org/10.1523/JNEUROSCI.0253-22.2022

Introduction

Children with hearing impairment have an increased risk for developing other disabilities, such as autism spectrum disorder (ASD). Hearing impairment might contribute to ASD core symptoms by interfering with language development, communication, social interaction, and overall quality of life (Kancherla et al., 2013; Do et al., 2017). Approximately 1 in 59 children with hearing loss receives school-based services for ASD, which is a much higher incidence than the 1 in 110 children with normal hearing reported to have ASD (Szymanski et al., 2012). It is difficult to disambiguate the effects of ASD from the effects of hearing loss and communication when both are present (Garreau et al., 1984; Roper et al., 2003). Previous studies found peripheral auditory system deficits in ASD children. For example, auditory brainstem response (ABR) wave I latencies were significantly delayed in an ASD group, suggesting peripheral auditory nerve (AN) dysfunction (Rosenhall et al., 2003). ASD children also show a reduction in otoacoustic emissions at the mid-frequency region compared with age-matched controls, indicating an abnormality of outer hair cell (OHC) activity (Bennetto et al., 2017).

Although previous observations support the hypothesis that central auditory processing abnormalities and structural/functional alterations contribute to ASD deficits, the direct impact of peripheral auditory system abnormalities on ASD symptoms is largely unknown (Rojas et al., 2011; Edgar et al., 2015; Rotschafer and Cramer, 2017; Scott et al., 2018; Smith et al., 2019). Importantly, accumulating evidence demonstrates that peripheral auditory system deficits, for example, dysfunction/damage of peripheral AN or inner hair cells (IHCs), contribute to changes observed in higher levels of the central auditory system (Chambers et al., 2016; Salvi et al., 2017; Schrode et al., 2018; Parthasarathy et al., 2019; Auerbach et al., 2021). These changes may contribute to auditory hypersensitivity, or hyperacusis, which is defined as unusual intolerance of ordinary environmental sounds and is commonly seen in ASD patients (Knipper et al., 2013; Hickox and Liberman, 2014; Chambers et al., 2016; Salvi et al., 2017; Amir et al., 2018). Given that ASD behaviors are linked to deficits at multiple levels of the nervous system (Amaral et al., 2008; Ha et al., 2015), it is challenging to distinguish the contribution of peripheral AN dysfunction to communication deficits and other ASD-like behaviors from the contributions of dysfunction at higher levels of the auditory pathway. Therefore, animal models of human ASD with a well-characterized peripheral auditory component are vitally needed to advance our understanding of the link between peripheral auditory impairment and ASD-related behaviors.

MEF2C belongs to the myocyte enhancer factor 2 (MEF2) subfamily of the MADS (MCM-agamous-deficiens-serum response factor) gene family, which is produced in several types of neurons and plays an important regulatory role in neuronal differentiation and synapse density in the developing cortex (Leifer et al., 1993; Harrington et al., 2016; Tu et al., 2017). Human *MEF2C* haploinsufficiency syndrome (MCHS), often caused by gene microdeletion or point mutation, is a newly described neurodevelopmental disorder with common symptoms that include ASD, absence of speech, hyperactivity, seizures, and intellectual disability. Studies of MCHS patients have identified numerous novel mutations in *MEF2C*, with many clustering in the DNA binding and dimerization domains and producing loss of DNA binding (Harrington et al., 2020). Based on these findings, we generated a DNA binding-deficient global *Mef2c* heterozygous mouse model of MCHS (*Mef2c*-Het mice). These mice exhibit numerous ASD-like behaviors, such as reduced ultrasonic vocalizations in a social context, social interaction deficits, hyperactivity, repetitive behavior, and reduced sensitivity to painful stimuli (Harrington et al., 2020). This mouse model of syndromic autism provides a means to directly investigate the relationship between peripheral AN dysfunction and ASD behaviors. Here we report that this mouse model of human MCHS has functional impairments of the AN at the physiological, cellular, and molecular levels. Further, our findings highlight the importance of immune cells and non-neuronal elements as regulatory factors in auditory impairment in ASD.

Materials and Methods

Animals

All aspects of animal research were conducted in accordance with the guidelines of the Institutional Animal Care and Use Committee of the Medical University of South Carolina. CBA/CaJ mice, originally purchased from The Jackson Laboratory, were bred in a low-noise environment at the Animal Research Facility at Medical University of South Carolina. *Mef2c*$^{+/-}$ (*Mef2c*-Het) mice were generated as described previously (Harrington et al., 2020). Briefly, this global heterozygous *Mef2c* mutant line was established by crossing exon 2 floxed *Mef2c* mice with *Prm1*-Cre mice (#003328; The Jackson Laboratory) to create a constitutive *Mef2c* loss-of-function allele (*Mef2c*$^{+/\Delta exon2}$). The *Prm1*-Cre transgene was subsequently removed during repeated backcrossing to C57BL/6J WT mice. This global heterozygous mutant impacts the Mef2c DNA binding function, but not the protein expression. In *Mef2c* Het mice, the germline-transmitted *Mef2c* heterozygous loss-of-function allele was generated by crossing Prm1-Cre (sperm expression) males with females having floxed *Mef2c* exon 2, which encodes a portion of the MADS/MEF2 domains. Removal of exon 2 allows for in-frame splicing of exons 1-3, producing a near full-length *Mef2c* open reading frame that lacks only the portion encoding the DNA binding/dimerization domain, similar to the MCHS missense mutations observed in patients. *Mef2c* conditional heterozygous mice were generated by crossing *Mef2c-flox* mice with macrophage-selective Cre-expressing transgenic mice (*Cx3Cr1*$^{creER/creER}$; The Jackson Laboratory #021160) to generate *Mef2c*$^{flox/+}$; *Cx3cr1-Cre* mice (*Mef2c cHet*^{Cx3cr1} mice) that were compared with their flox-negative littermates (control mice).

All mice received food and water *ad libitum* and were maintained on a 12 h light/dark cycle. Mice with signs of obstruction or infection in the external ear canal or middle ear were excluded. All mice of both sexes underwent measurement of auditory physiology and at least one other molecular or cellular assay, including RNA sequencing, immunohistochemistry, and transmission electron microscopy (TEM) (see detailed information of these assays below).

Auditory physiology

Cochlear and AN functions were measured using the cochlear microphonic (CM), and the ABR. The CM is used as a proxy of mouse cochlear health (Cheatham et al., 2011). The CM is an AC receptor potential with electromechanical origins that is sensitive to changes in the endocochlear potential and hair cell (HC) loss. The CM represents the functional sum of the HCs, basilar membrane, and strial effects. The CM is often considered a measure of OHC function, similar to otoacoustic emissions, such that damage to the OHCs and hearing loss result in reduced CM amplitude. The ABR wave I was used to assess several metrics of the peripheral AN function via both averaged and single-trial ABR recording (for detailed information, see sections below). Averaged recording provided estimates of ABR wave I threshold and suprathreshold measurement and single-trial ABR recordings provided estimates of neural synchrony as in our previous reports in mouse models (Jyothi et al., 2010; Panganiban et al., 2018, 2022; McClaskey et al., 2020). Suprathreshold estimates of AN peak response amplitudes and latency, and neural synchrony (phase-locking value PLV) were acquired. These

suprathreshold measures of the ABR have been associated with speech recognition in noise (Harris et al., 2018, 2021).

For measurements of auditory function, WT and *Mef2c*-Het littermates (both males and females) at postnatal day (P) 16, 2-3, and 6-7 months were anesthetized via an intraperitoneal injection of a cocktail containing 20 mg/kg xylazine and 100 mg/kg ketamine. Auditory tests were performed in a sound-isolation booth. CM and ABR recordings were performed using a Tucker Davis Technologies RZ6 multi- input/output (I/O) Processor. Equipment for auditory functional measurements (CM and ABR) was calibrated before use with TDT RPvdsEx software (Tucker Davis Technologies) and a model 378C01 ICP microphone system provided by PCB Piezotronics. In a closed-field setup, sound stimuli were delivered into the ear canal via a 3- to 5-mm-diameter tube.

CM. The CM was elicited by a 100 ms 4 kHz tone-burst with a 10 ms $\cos^2$ rise/fall time. Sound levels were reduced in 10 dB steps, from 120 to 70 dB SPL. Since the CM reflects a presynaptic potential, stimuli had a high repetition rate (5 ms gap between presentations) to reduce the influence of the neural response. The active electrode (channel 1) was placed around the bulla of the ear for which the CM was measured and the inverting electrode subdermally into the scalp at the vertex and between the ears. The ground electrode was placed at the hindlimb. The CM was recorded using 600 trials. Data processing was performed in MATLAB using custom scripts and EEGLAB. The CM was measured in the frequency domain as the power of the signal at the eliciting stimulus frequency (4 kHz).

ABR: threshold measures. ABRs were evoked at frequencies of 4, 5.6, 11.3, 16, 22.6, 32, 40, and 45.2 kHz with 5 ms tone pips with 0.5 ms $\cos^2$ rise/fall times delivered at 31/s using a Tucker Davis Technologies system III with a RP2.1 enhanced real-time processor. For ABR recordings, the active electrode (channel 1) was placed into the scalp subdermally at the vertex and between the ears, and the inverting electrode around the bulla of the ear for which the ABR was measured. The ground electrode was placed at the hindlimb. Sound levels were reduced by 5 dB steps, from 90 to 10 dB SPL. The average ABR waveform for each level tested consisted of 256 trials. Wave I thresholds were determined visually for each mouse as the lowest level that elicited an ABR response, as determined by at least two experienced reviewers. Thresholds were then averaged at each frequency across groups, and the mean ± SEM was calculated and plotted using Origin 6.0 software (OriginLab) or GraphPad Prism 9 (GraphPad Software).

ABR: Suprathreshold measures. Suprathreshold wave I peak amplitudes were measured. Peak-to-peak wave I amplitudes were measured from the positive peak to the following negative deflection using a custom MATLAB (The MathWorks) script, in which the experimenter selected peaks while being blinded to genotype. Our recent report (McClaskey et al., 2020) identified a break point in the growth of wave I at ~75 dB SPL. Therefore, levels above this break point were classified as suprathreshold and reflected the response of a larger contingent of AN fibers with various thresholds, including higher threshold fibers hypothesized to be important for speech recognition.

The procedure for continuous single-trial recording of ABR was modified from our recent report (McClaskey et al., 2020; Panganiban et al., 2022). Stimuli were 1.1 ms in duration with 0.55 ms $\cos^2$ rise/fall times and were presented at a rate of 21/s at the levels of 5-90 dB SPL in 5 dB increments. At least 500 tone pips of each sound level were presented. ABR responses were stored and processed offline in MATLAB using the EEGlab toolbox (Delorme and Makeig, 2004) and the ERPlab extension (Lopez-Calderon and Luck, 2014). Continuous data were bandpass filtered between 100 and 3000 Hz using an eighth-order Butterworth filter. Data were then epoched from −3 to 11 ms relative to stimulus onset and baseline corrected by subtracting the mean value in the pre-stimulus window of −3 to −1 ms. Epochs with voltages exceeding ±5 μV were rejected, and the remaining epochs were visually inspected for excessive movement or other artifacts. Artifact-free trials were saved in the single-trial form in EEGLAB (https://sccn.ucsd.edu/eeglab/index.php) and as a trial-averaged ABR waveform in ERPLAB (https://sccn.ucsd.edu/eeglab/index.php). Wave I was visually identified as the first major positive deflection following stimulus onset. PLV was calculated from the single-trial-level data.

PLV, also known as intertrial coherence, is the length of the vector that is formed by averaging the complex phase angles of each trial at each frequency and was obtained via time-frequency decomposition of the single-trial-level data. With increasing stimulus level, first-spike latencies decrease and become more consistent across AN fibers (Heil and Irvine, 1997; Heil, 2004); this decrease in jitter is hypothesized to improve timing across trials, resulting in stronger PLV. Time-frequency decomposition was performed with Hanning FFT tapers via EEGlab's newtimef() function, using 16 linearly spaced frequencies from 190 to 3150 Hz. PLV at each time point and each frequency was then calculated by taking the absolute value of the complex intertrial coherence output of the newtimef() function, using the following equation, in which F_k (f, t) is the spectral estimate of trial k at frequency f and time t as follows:

$$PLV(f,t) = \frac{1}{n}\sum\nolimits_{k=1}^{n} \frac{F_k(f,t)}{|F_k(f,t)|}$$

The maximum PLV between 250 and 2500 Hz in the 2 ms window surrounding the wave I peak was then measured as PLV.

AN tissue collection and total RNA isolation

Throughout the paper, the term "auditory nerve" (AN) refers to the peripheral part of the VIII nerve extending from synapses with HCs in the organ of Corti to the main nerve trunk within the modiolus and extending into the internal auditory canal. AN tissues were collected at their designated endpoints using both cochleae from each mouse. Microdissections were performed to isolate the AN from the rest of the cochlear structures, taking care to preserve peripheral fibers. Samples were created by pooling ANs collected from either one mouse (aging study) or 2 mice (*Mef2c* deficiency study). Total RNA was isolated using the RNeasy Plus Mini Kit (QIAGEN) per the manufacturer's instructions. Quality of each total RNA preparation was assessed by 4200 TapeStation (Agilent Technologies). Low-quality samples showing degradation or contamination were excluded.

RNA sequencing (RNA-seq)

RNA-seq analysis of CBA/CaJ mouse AN development (NCBI accession GSE133823) and aging (NCBI accession GSE141865) have been described previously (Panganiban et al., 2022). For the developmental study, P3, P7, P14, P21, and adult AN samples were analyzed; for the aging study, aged adult (2.5 years) and young adult (2 months) AN samples were analyzed. RNA-seq analysis of the effects of Mef2c deficiency was done using P21 WT and *Mef2c*-Het mice (both sexes) and four biological replicates of each sample type. Sequencing libraries were prepared at the Medical University of South Carolina Translational Science Lab. Polyadenylated RNA was captured from 50 ng of total RNA per sample, and libraries were prepared using the NEBNext Poly(A) mRNA Magnetic Isolation Module and NEBNext Ultra II Directional RNA Library Prep Kit for Illumina (New England Biolabs). Paired-end sequencing was done at the Vanderbilt VANTAGE core laboratory (Vanderbilt University) to a depth of 25 million reads/library using an Illumina NovaSeq 6000. Sequencing data were analyzed using Partek Flow software. Reads were aligned to mouse genome assembly mm10 with an implementation of STAR (Spliced Transcripts Alignment to a Reference) (Dobin et al., 2013) and quantified to annotation model (Partek E/M) using mm10. Calculation of fold change and adjusted p value (FDR step-up) was done with DESeq2 (Love et al., 2014). Raw sequencing data (fastq files) and comparison results for the *Mef2c*-Het study are archived in NCBI Gene Expression Omnibus (accession GSE182857).

Comparative analysis of RNA-seq data

For evaluation of ASD-related gene expression during AN development: (1) comparison data were obtained for GSE133823; and (2) ASD-related genes were compiled from Simons Foundation Autism Research Initiative (SFARI) database Categories 1-4, which comprise genes with high confidence through genes with minimal evidence (https://gene.sfari.org). Genes differentially expressed during development were defined as adjusted p value (FDR step-up) <0.10

Table 1. Antibodies used in the study

	Host	Company	Catalog #	Concentration
Primary antibody				
Anti-MEF2C	Rabbit	Abcam	EPR19089-34	1:250
Anti-IBA1	Rabbit	Wako	019-19741	1:200
Anti-MBP	Mouse	Abcam	Ab24567	1:250
Anti-FABP7	Rabbit	Acris	AP21789PU-N	1:200
Anti-GFAP	Mouse	Millipore	MAB360	1:300
Anti-CALB2 (calretinin)	Goat	Swant	CG1	1:1000
Anti-Class III β-tubulin	Rabbit	Santa Cruz Biotechnology	SC-68377	1:200
Anti-peripherin	Mouse	Chemicon	AB1530	1:150
Anti-NDUFB8	Mouse	Invitrogen	Ab_2532232	1:100
Anti-CALB1	Polyclonal rabbit	Cell Signaling	13176S	1:100
Anti-KIR4.1	Rabbit	Alomone Labs	PC035AN0802	1:200
Anti-CTBP	Mouse	BD Biosciences	612044	1:100
Secondary antibody				
Biotinylated anti-goat IgG	Horse	Vector Laboratories	BA-9500	1:100
Biotinylated anti-rabbit IgG	Horse	Vector Laboratories	BA-1100	1:100
Biotinylated anti-mouse IgG	Goat	Vector Laboratories	BA-9200	1:100
Anti-biotin dyes				
Fluorescein avidin DCS	NA	Vector Laboratories	A-2011	1:100
Texas Red avidin D	NA	Vector Laboratories	A-2006	1:100

and absolute fold change >1.5 for P21 versus P3 AN. Commonality between developmentally regulated genes, ASD-related genes, and macrophage/inflammation-related genes was done by Venn analysis using gene symbols as input. For RNA-seq analysis of *Mef2c*-Het compared with WT AN, differential expression was also defined as adjusted p value (FDR step-up) <0.10 and absolute fold change >1.5, identifying 258 genes. Biological process enrichment was conducted with ToppFun (Chen et al., 2009); enrichment results were refined and the interactive graph generated by REVIGO (Supek et al., 2011). To determine whether genes affected by Mef2c deficiency were also affected in aged AN, comparison data were obtained for the aging AN RNA-seq study (accession GSE141865), and statistical measures for the 258 genes affected in *Mef2c*-Het AN were reviewed. Significant difference for aged adult versus young adult AN was defined as adjusted p value (FDR step-up) <0.10, identifying 19 of the 258 genes.

Immunohistochemistry and lectin histochemistry

Immunohistochemical procedures were modified from previous studies (Panganiban et al., 2018, 2022). After endpoint physiological recordings, mouse cochleae were collected and immediately fixed with 4% PFA solution in 1× PBS for 2 h at room temperature and decalcified with 0.12 M EDTA at room temperature for 1-2 d. To prepare mouse cochlea sections, cochleae were embedded in the Tissue-Tek OCT compound and sectioned at a thickness of ~12 µm. For whole-mount preparations of mouse cochlear tissues, the ANs, cochlear lateral wall, and organs of Corti were isolated separately based on the experimental plans (e.g., to count HCs, or to evaluate the strial microvasculature).

Primary and secondary antibodies used for immunohistochemistry are listed in Table 1. Staining was performed by either indirect method using biotinylated secondary antibodies conjugated with fluorescent avidin (Vector Labs) or direct method using primary antibodies conjugated to AlexaFluor dyes (Thermo Fisher Scientific). Nuclei were counterstained using propidium iodide or DAPI.

A lectin histochemical approach was used to visualize the blood vessel system in mouse strial vascularis modified from previous studies (Meyer et al., 2008; Shi, 2011). For whole-mount preparations of mouse cochlear lateral wall tissues, the fluorescent lectin Gs-IB4 AlexaFluor-488 was diluted in PBS with 0.1% $CaCl_2$ (1:100), and the tissue was incubated overnight at 4°C.

Slice and confocal image stacks were collected using a Zeiss LSM 880 NLO with Airyscan and ZEN acquisition software (Carl Zeiss). Images were processed using ZEN 2012 Blue Edition (Carl Zeiss Microscopy) and Adobe Photoshop CC (Adobe Systems). Quantitative analysis of macrophage size and volume was done with the Surface module of IMARIS (IMARISx64 9.3.1) with Z-stack images collected via LSM 880 NLO.

TEM

Samples were prepared for TEM using procedures modified from previous publications (Lang et al., 2016). Briefly, deeply anesthetized mice were cardiac perfused with 15 ml of a fixative solution containing 4% PFA and 2% glutaraldehyde in 0.1 M PB, pH 7.4. The same fixative solution was used to perfuse the excised cochleae through the round window and for further immersion overnight at 4°C. Cochleae were decalcified using 0.12 M EDTA solution at room temperature for 2-3 d with a magnetic stirrer. Cochleae were then fixed using a solution containing 1% osmium tetroxide and 1.5% ferrocyanide for 2 h in the dark and then dehydrated and embedded in Epon LX 112 resin. Semithin sections for pre-TEM observation of AN orientation were cut at 1 µm thickness and stained with toluidine blue. Once a coronal plane for a given cochlear turn was seen, ultrathin sections at 70 nm thickness were cut and stained with uranyl acetate and lead citrate. Ultrathin sections were examined using a JEOL JEM-1010 transmission electron microscope (JEOL).

Characterization of spiral ganglion neuron (SGN) pathology, myelination, and mitochondrial abnormity in AN

Quantitative analyses of ultrastructural alteration in myelin and mitochondria and examination of aging-like neuronal pathology were conducted on TEM graphs collected from the middle portions of cochleas. A myelin sheath was classified as abnormal if it exhibited at least two areas with degenerative myelin features. Such features included splitting, folded or collapsed lamella, or balloon-like features (Xing et al., 2012; Helvacioglu and Dagdeviren, 2019). A mitochondria was classified as dysfunctional if it exhibited disrupted cristae or loss of condensed cristae (Perkins et al., 2020; Joubert and Puff, 2021) (Fig. 5*M*). A SGN cell body was classified as exhibiting an aging-like feature if it contained a cluster of at least two lipofuscin-accumulated granules (aging pigment; Fig. 5*F*) (Sulzer et al., 2008; Vila, 2019). For quantitative analysis of abnormal myelin and aging-like neuronal pathology, 4 animals per genotype and 17-90 neurons per animal were examined. For quantitative analysis of dysfunctional mitochondria, 3 WT and 4 *Mef2c*-Het mice were analyzed and 62-249 mitochondria per AN were examined in randomly selected AN axons.

Experimental design and statistical analyses

Experimental plans were designed to achieve a statistical power of ≥80% and a significance level of ≤0.05 (de Aguilar-Nascimento, 2005). Sample sizes (n) are indicated in each figure legend or in Results. Sample size for

physiological measurements (e.g., ABR wave I threshold, wave I amplitude and latency) was estimated based on effect sizes obtained from observed means and SDs of preliminary data and from previous studies by our laboratory and our collaborators (Xing et al., 2012; Lang et al., 2016; Panganiban et al., 2018, 2022; Harrington et al., 2020; McClaskey et al., 2020). For RNA-seq, prior analyses of mouse AN demonstrated that a sample size of $n = 3$ was sufficient for robust detection of genes differentially expressed with an effect size of 1.5-fold and false discovery rate <10% (Lang et al., 2016; Panganiban et al., 2022). For datasets other than RNA-seq, data distribution was tested using either Shapiro–Wilk or Kolmogorov–Smirnov tests for normality. The appropriate parametric or nonparametric tests were then used for the AN functional and structural data. Statistical software and packages used in this study included DeSeq2 (Love et al., 2014), Microsoft Excel, R version 3.5.2 (R Foundation for Statistical Computing 2019), and GraphPad Prism 8 (GraphPad Software). Type III ANOVA was used for analysis of ribbon synapse count in the AN. Student's *t* test and/or linear mixed-effects regression models were used for analyses of ABR wave I threshold, amplitude growth functions, PLV and CM. Linear regression models were used for analyses of the slope of ABR wave I amplitude growth functions. Linear mixed-effects regression and linear regression model analyses are performed in R using the lme4 package (Bates et al., 2015). For the Mann–Whitney *U* test, which was applied to the analyses of the averaged cellular or subcellular structures using ultrastructural and immunohistochemical evaluation, a *p* value of ≤ 0.05 was considered significant. For analyses of the cellular area and volume in the cochlear macrophages, unpaired, two-tailed *t* test with Welch's corrections was used. For differential expression analyses of complete RNA-seq datasets, a *p*-adjusted (FDR step-up) value of ≤ 0.10 and absolute fold change >1.5 was considered significant; for analyses that examined subsets of RNA-seq data (<1000 genes), *p*-adjusted (FDR step-up) value of ≤ 0.10 was considered significant. Detailed information for statistical analyses is included in supplementary data tables designated as Extended Data Figures 1-1, 1-2, 2-1, 3-1, 3-2, 4-1, 5-1, 6-1, 7-1, and 8-1.

Results

Numerous ASD risk genes, including *Mef2c*, are differentially expressed during mouse peripheral AN development

The ASD risk gene *MEF2C* is highly expressed in several areas of the early developing brain (e.g., in differentiated forebrain neurons within the neocortex and dentate gyrus) and maintains its expression in multiple types of postmitotic neurons, such as glutamatergic neurons, GABAergic neurons, and Purkinje cells (Leifer et al., 1993, 1997; Lyons et al., 1995; Speliotes et al., 1996; Harrington et al., 2016). We hypothesized that *Mef2c*, and possibly other ASD risk genes, may play a role in peripheral AN development. To test this hypothesis, we performed an analysis to determine whether ASD risk genes were regulated during AN development. A list of ASD risk genes was obtained from the SFARI database (Categories 1-4; https://gene.sfari.org), and an RNA-seq dataset profiling gene expression during AN development was obtained (NCBI GEO accession GSE133823). Evaluation of expression data for the 671 ASD risk genes found that 319 (48%) were differentially expressed during AN development (Fig. 1*A*). Similar to observations in the CNS, *Mef2c* was highly expressed in the mouse AN in early postnatal development periods (e.g., P3), but then it undergoes downregulation during hearing onset. It then maintains a measurable level from P21 to adulthood (Fig. 1*B*,*C*). Interestingly, among differentially expressed genes, *Pik3cg* is a *Mef2c* gene target and plays a regulatory role in plasticity of nucleus accumbens in a cocaine-exposed animal model (Pulipparacharuvil et al., 2008).

To validate the *Mef2c* expression findings, immunostaining was performed for MEF2C together with markers of SGNs and macrophage/microglia, revealing that multiple cell types in AN and cochlea expressed MEF2C protein (Fig. 1*D*–*G*). These cell types include Type I SGNs (Fig. 1*D*) (Sekerková et al., 2005; Jyothi et al., 2010), high- and mid-spontaneous rate (SR) SGNs ($CALB2^+$ and $CALB1^+$, respectively; Fig. 1*E*,*F*) (Petitpré et al., 2018; Shrestha et al., 2018; Sun et al., 2018), and macrophages ($IBA1^+$; Fig. 1*G*) (Brown et al., 2017). Low SR-SGN express either none or a very limited level of two calcium-binding proteins, calbindin (CALB1) and calretinin (CALB2), which are highly expressed in mid-and high-SR fibers, respectively. We observed some MEF2C-positive SGNs that were negative for CALB2 and CALB1 (red), suggesting that low-SR SGNs are also MEF2C-expressing neurons (Fig. 1*E*,*F*). MEF2C-expressing cells were also seen in and around $CD31^+$ blood vessels within the strial vascularis and AN (Fig. 1*I*,*J*,*L*,*M*) (Lang et al., 2016). In addition, MEF2C was highly expressed in bone-forming cells around the cochlear lateral wall and AN (Fig. 1*H*,*K*–*M*).

Mef2c deficiency results in a mild reduction of hearing sensitivity in young adult animals

ABR wave I thresholds were measured at P16 and in young adult (2-3 months old) *Mef2c*-Het mice and their WT littermate controls for evaluation of hearing sensitivity. In agreement with a previous study in another mouse strain, ABR wave I threshold was lower in young adult C57BL/6J WT mice compared with animals at P16 (shortly after hearing onset Fig. 2*C*,*D*) (Song et al., 2006) *Mef2c*-Het mice showed threshold changes in young adults at 2-3 months. A significant elevation of ABR wave I thresholds was observed at most middle and low frequencies in young adult *Mef2c*-Het mice compared with their littermate WT controls (Fig. 2*D*). Elevated thresholds ranged from 8 to 20 dB SPL (Extended Data Fig. 2-1), suggesting a mild reduction of hearing sensitivity in young adult *Mef2c*-Het mice. No significant difference in ABR threshold was identified between male and female animals at age 2-3 months, suggesting sex is not an effect modifier for hearing sensitivity in *Mef2c*-Het mice (Fig. 2*E*).

MEF2C deficiency results in reduced neural synchrony and AN activity

To further evaluate peripheral auditory function, we measured suprathreshold AN function using the PLV. PLV is measured across single-trial ABR recording (Harris et al., 2018, 2021; McClaskey et al., 2020), and it quantifies the consistency of the phase of the response across individual trials (synchrony) within a given frequency range. The amplitude of the ABR is dependent on two independent factors: the number of neurons actively engaged by the stimulus and the synchrony of the response across trials (PLV). Factors that affect synchrony may therefore result in a smaller ABR amplitude despite a relatively preserved contingency of AN fibers. Similarly, a loss of AN fibers with preserved synchrony in the remaining fibers would result in a smaller peak amplitude. As shown in Figure 3*A*, *B*, PLV was quantified at suprathreshold levels (60 dB SPL and above) and a linear mixed-effects regression was performed with stimulus level and genotype as fixed factors and mouse as a random factor, with stimulus level nested within the mouse. Stimulus level was a significant predictor of PLV [$B = 0.014$, $t_{(70)} = 9.861$, $p < 0.001$], with PLV increasing with stimulus level for both genotypes. Most importantly, mouse genotype was a significant predictor of PLV [$B = -0.375$, $t_{(75.76)} = -3.241$, $p = 0.001$], with PLV higher for WT mice than for *Mef2c*-Het mice. There was also a significant interaction between mouse genotype and stimulus level [$B = 0.004$, $t_{(70)} = 2.84$, $p = 0.006$],

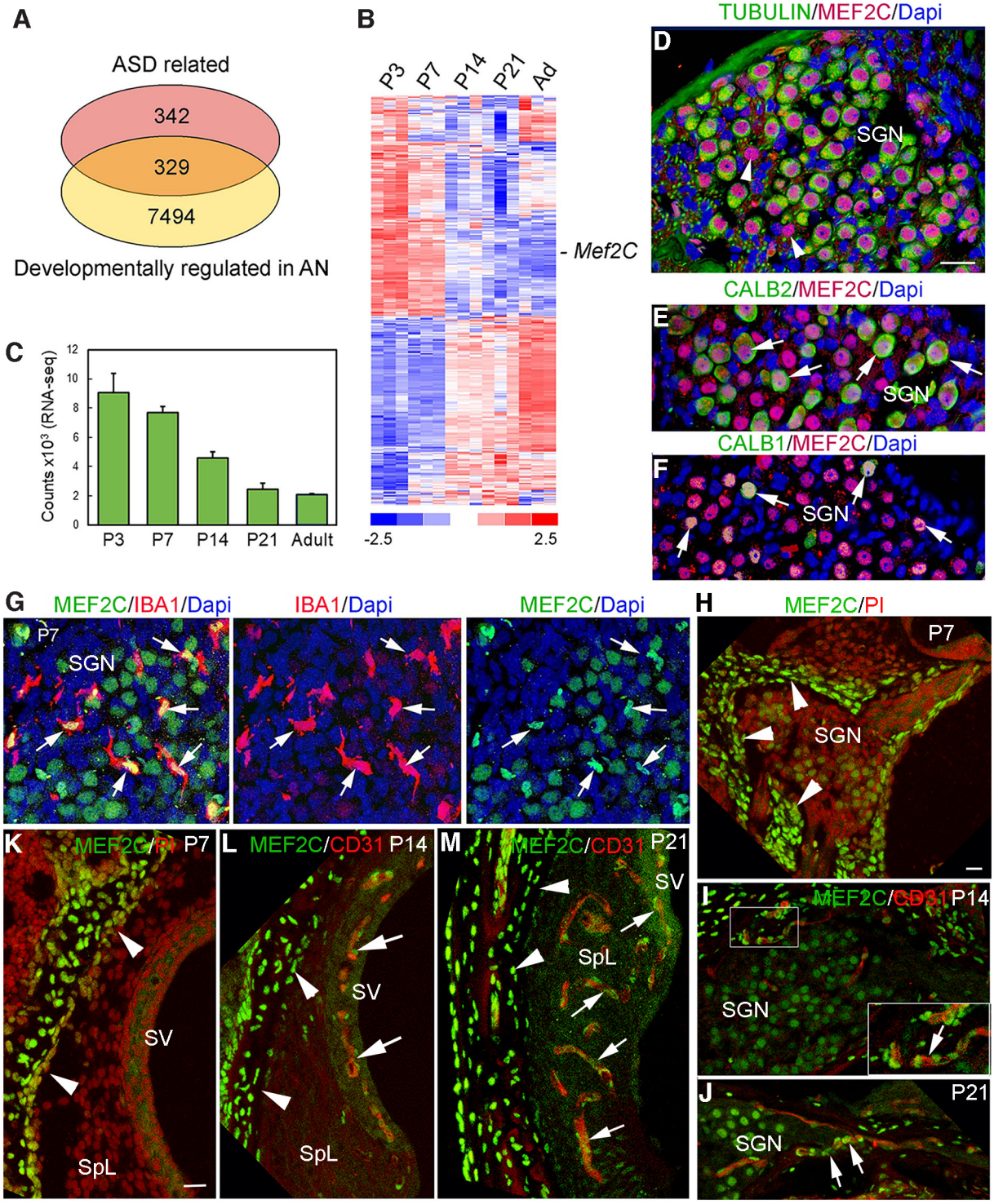

Figure 1. Expression of ASD risk genes in the mouse peripheral auditory system. ***A***, Venn diagram depicting overlap between (1) ASD-risk genes and (2) genes regulated during AN development. The list of ASD-related genes differentially expressed in mouse AN during development is included in Extended Data Figure 1-1. ***B***, Heatmap of ASD-risk genes differentially expressed in mouse AN during development, including *Mef2c*. ***C***, Mef2c mRNA expression is highest in AN in postnatal stages preceding hearing onset (around P12). Graph represents RNA-seq standardized counts (for detailed information, see Extended Data Fig. 1-2). ***D***, ***E***, Detection of MEF2C protein (purple) in Type I SGNs (TUBULIN$^+$; green in ***D***), high-SR SGNs (CALB2$^+$, green in ***E***), and mid-SR SGNs (CALB1$^+$, green in ***F***) in young adult mouse AN. Arrowheads indicate MEF2C$^+$/ TUBULIN$^-$ Type II SGN-like cells. ***G***, Expression of MEF2C (green) in macrophages in mouse P7 AN. Macrophages were identified by immunostaining for Iba1 (red). Nuclei were stained with DAPI (blue). ***H–J***, Images represent MEF2C-expressing cells present around a blood vessel in AN (***I***,***J***; arrows) and cochlear lateral wall (***L***,***M***; arrows) and areas near bone-forming cells in postnatal developing cochlea (***H***,***K–M***; arrowheads). Scale bars: ***D*** (applies to ***E–G***), ***H*** (applies to ***I***,***J***), ***K*** (applies to ***L***,***M***), 20 μm.

indicating that the PLV of *Mef2c*-Het mice decreased with decreasing stimulus level to a stronger degree than for WT mice. In addition, *post hoc* independent *t* tests with Bonferroni correction showed that the difference between groups was significant at 60 dB SPL, where the PLV of *Mef2c*-Het mice (mean = 0.337) was lower than the PLV of WT mice (mean = 0.575) [$t_{(10)} = 3.402$, $p = 0.007$, Cohen's $d = 2.152$]. Together, these analyses revealed that Mef2c deficiency results in reduced neural synchrony at

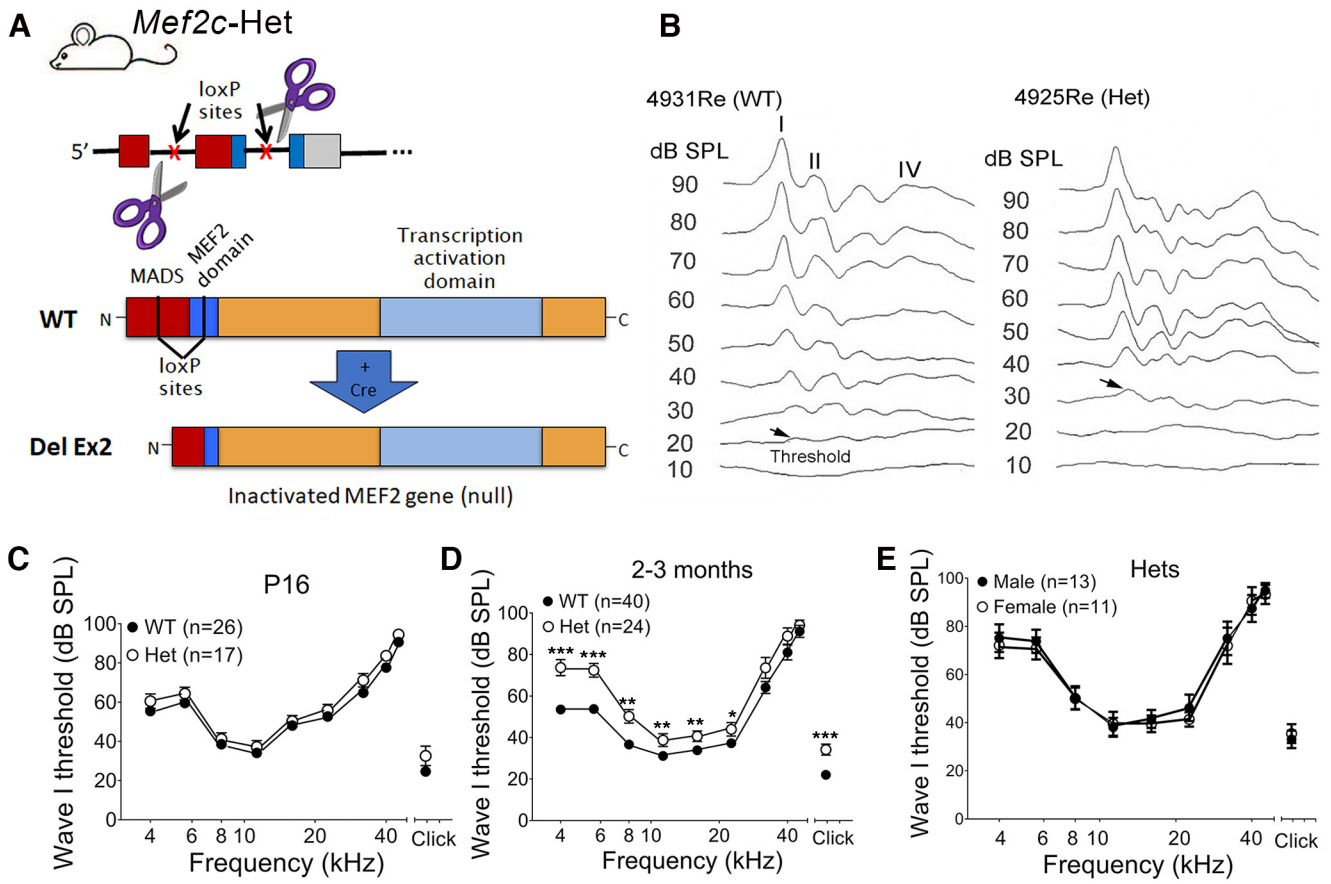

Figure 2. MEF2C deficiency causes a mild reduction of hearing sensitivity in young adult mice. ***A***, Schematic represents mouse *Mef2c* gene exons 1-3 and the approximate region eliminated (exon 2 [Ex2]) in the global heterozygous *Mef2c* mutant (*Mef2c*-Het). Exon 2 encodes a large part of the MADS/MEF2 domains (Harrington et al., 2020). ***B***, ABRs to click stimuli were recorded in a young adult *Mef2c*-Het mouse and a WT littermate control (WT). ABR waveforms from I to IV and an elevated ABR wave I threshold (arrows) in *Mef2c*-Het mice are shown for two representative young adult animals. ***C–E***, The averaged ABR wave I thresholds are shown in WTs and *Mef2c*-Het mice aged P16 (***C***) and 2-3 months (***D***). Significant threshold shifts were present in *Mef2c*-Het animals compared with littermate controls (WTs) in both young adult groups (ABR wave I thresholds are mean ± SEM). $^{*}p < 0.05$; $^{**}p < 0.01$; $^{***}p < 0.001$; unpaired *t* test with Welch's correction. For detailed statistical analysis information, see Extended Data Figure 2-1. ABR threshold difference was not identified between a group of *Mef2c*-Het mice and littermate controls (***E***).

certain suprathreshold levels in the AN of young adult animals. To further characterize the AN dysfunction, we measured ABR wave I amplitude I/O functions (or amplitude growth functions), which allowed for evaluation of AN function at suprathreshold levels, in WT and *Mef2c*-Het mice (Fig. 3*C*,*D*). Linear mixed-effects regression revealed that stimulus level was a significant predictor of amplitude, with amplitude increasing with stimulus level for both genotypes. There was a significant interaction between mouse genotype and stimulus level at 8 kHz, demonstrating that amplitudes increase more with increasing stimulus level in WTs compared with *Mef2c*-Het mice (for detailed information, see Extended Data Fig. 3-2; Fig. 3*C*). In addition, the linear effects model analysis revealed significant effects of genotype on slope of the wave I amplitude growth function for both 8 and 11 kHz (Fig. 3*C*,*D*; Extended Data Fig. 3-2), indicating that AN activity was reduced at higher levels in *Mef2c*-Het mice. These observations further confirm the decline of suprathreshold AN activity in young adult *Mef2c*-Het mice.

MEF2C deficiency leads to glial dysfunction in AN of young adult animals

To further elucidate the cellular and molecular changes that may contribute to these deficits, RNA-seq analysis was conducted on AN in *Mef2c*-Het mice at P21, a stage at which mouse ABR wave I threshold approximates the level of young adults (Song et al., 2006). As shown in Figure 4*A–D*, RNA-seq analysis of WT and *Mef2c*-Het mice AN identified 258 genes that were differentially expressed (fold change >1.5 and *p*adj <0.10) (Extended Data Fig. 4-1). Enrichment analysis of these genes showed that they were highly representative of neurogenic function, with the top 15 significant biological processes, including categories relating to glia cells, myelination, and other neural developmental processes. To clarify these findings, all significant biological processes were refined by eliminating redundant categories. This refinement revealed that there was a cluster of highly similar processes that were centrally linked to sensory perception of sound. This cluster included several processes relating to glial cell function and myelination and also processes relating to the development of tissues derived from mesenchymal cell lineages.

Proper glial cell development and function (e.g., myelination) are critical for AN structural and functional maturation (Panganiban et al., 2022). A small alteration in conduction velocity resulting from changes in myelin integrity may have significant effects on neuronal function, such as spike-time arrival and neural synchrony (Pajevic et al., 2014). Here our RNA-seq analysis of *Mef2c*-Het mice found that there was downregulation of numerous glial cell markers, several of which have established importance in other nervous systems. These markers were detected in several different types of glial cells in AN of *Mef2c*-Het mice (Fig. 4*D–F*). For example,

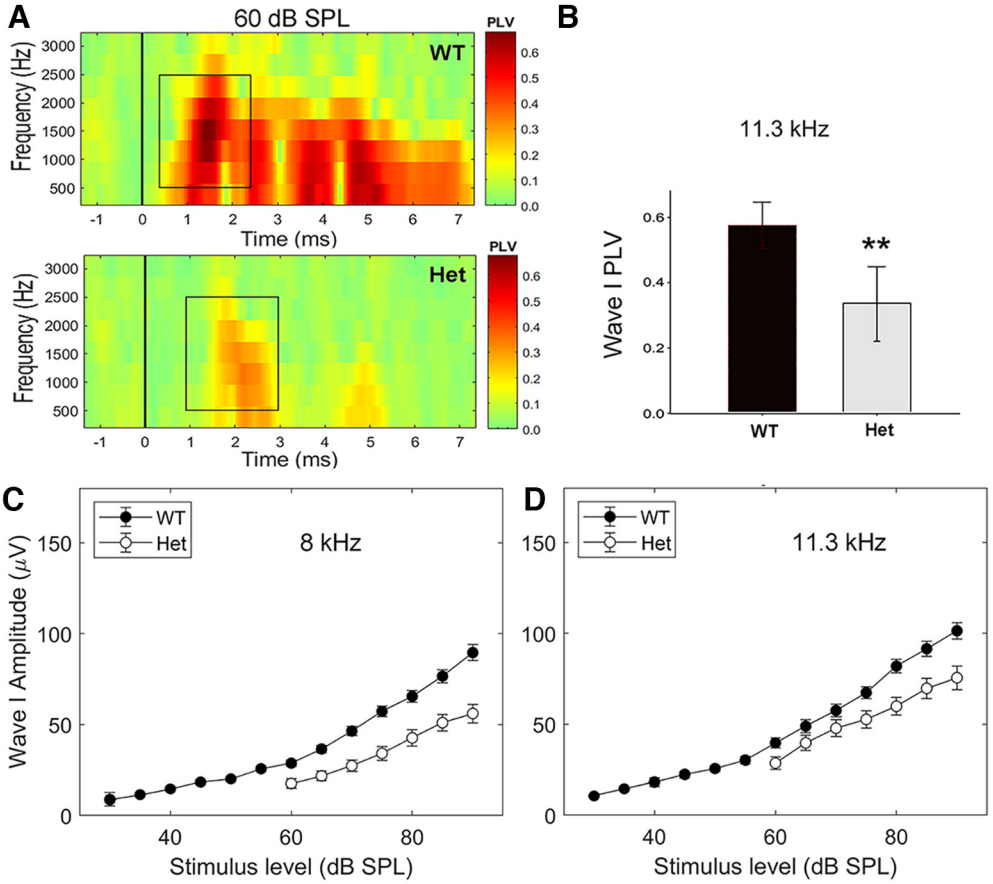

Figure 3. Reduced neural synchrony and AN activity in young adult *Mef2c*-Het mice. ***A***, ***B***, Synchrony of AN firing of *Mef2c*-Het mice was poorer than that in WT mice. PLV reflects uniformity of phase at a specific time and frequency across trials and has been used to measure synchronization in neural activity from mouse ABR data. In the heat-map images in ***A***, the *x* axis represents time (signal onset = 1 ms); the *y* axis represents frequency. Strength of PLV above baseline (green) is indicated by color (red). Independent *t* tests with *post hoc* Bonferroni corrections revealed that the difference between groups is most pronounced at 60 dB SPL, where the PLV of *Mef2c*-Het mice is significantly lower than the PLV of WT mice ($n = 6$ animals per group). $^{**}p < 0.01$. For detailed statistical information, see Extended Data Figure 3-1. ***C***, ***D***, ABR amplitude I/O functions at 8 and 11.3 kHz in WTs and *Mef2c*-Het mice. Note the reduced amplitudes of *Mef2c*-Het mice at high stimulus levels and a significant change in the slope of amplitude growth (from 75 to 90 dB SPL) compared with WT, suggesting a decline of auditory suprathreshold function ($p = 0.025$ and 0.005 for 8 and 11.3 kHz; for detailed statistical information, see Extended Data Fig. 3-2).

myelin proteolipid protein 1 (*Plp1*) was present in Schwann cells around AN axons within the osseous spiral lamina (OSL). MBP was located in satellite cells around SGNs and axons. Fatty Acid Binding Protein 7 (FABP7) was seen in satellite cells of a small subset of SGNs, Type II SGNs, which are often found in the periphery of the spiral ganglion. GFAP was expressed in the oligodendrocytes in the central AN process, which is located next to the glial transition zone (Fig. 4*F*). Ultrastructural examination of young adult AN myelin detected pathologies in *Mef2c*-Het mice (Fig. 4*G–J*). SGNs appeared normal in WT adult animals based on the neuronal cell bodies being completely enveloped by a thick, compact myelin sheath (Fig. 4*G*). In contrast, several features of degeneration were apparent in myelin sheaths of *Mef2c*-Het AN, including folded or collapsed lamella with balloon-like features (Fig. 4*H*), thinner lamellae, loose lamellae, or split myelin lamellae with discontinuities containing vacuole-like inclusions (Fig. 4*I*) in glial cell cytoplasm. Disorganization of myelin was evident both in SGNs with severe degenerative changes and also in SGNs with a relatively normal appearance. Disrupted myelin sheaths were also seen in AN processes within Rosenthal's canal and the osseous spiral lamina. Quantification of SGNs with myelin sheath abnormalities showed that occurrence was significantly increased in young adult *Mef2c*-Het mice compared with littermate WT controls. In 236 randomly selected SGNs from the middle turn sections of four WTs and 4 *Mef2c*-Het mice, 46 ± 4% of SGNs in *Mef2c*-Het mice showed abnormal myelin compared with only 24 ± 3% in WT controls ($p = 0.002$, Mann–Whitney *U* test; Fig. 4*J*).

MEF2C deficiency causes aging-like alterations in neurons and mitochondria in young adult AN

Ultrastructural observations of *Mef2c*-Het AN detected evidence of SGN degeneration, including a loss of SGNs (Fig. 5*A*) and the presence of apoptotic bodies within dying SGNs (Fig. 5*B*). To quantify the effects on neuronal cell number, we performed immunolabeling studies in *Mef2c*-Het and littermate controls at both young adult (2-3 months) and older (6-7 months) stages to detect βIII-tubulin, which has been previously shown to be highly expressed in Type I SGNs of the young adult mouse (Sekerková et al., 2005; Jyothi et al., 2010). Interestingly, statistical analysis of the findings did not reveal a significant difference in numbers of neuronal cells between *Mef2c*-Het and littermate controls at either the young adult stage (Fig. 5*C*) ($n = 3$ animals per group; $p > 0.05$, Mann–Whitney *U* test) or older adult stage (*Mef2c*-Het, $n = 5$; littermate WT control, $n = 7$; $p > 0.05$, Mann-Whiney *U* test). This suggests that the number of affected cells in *Mef2*-Het mice

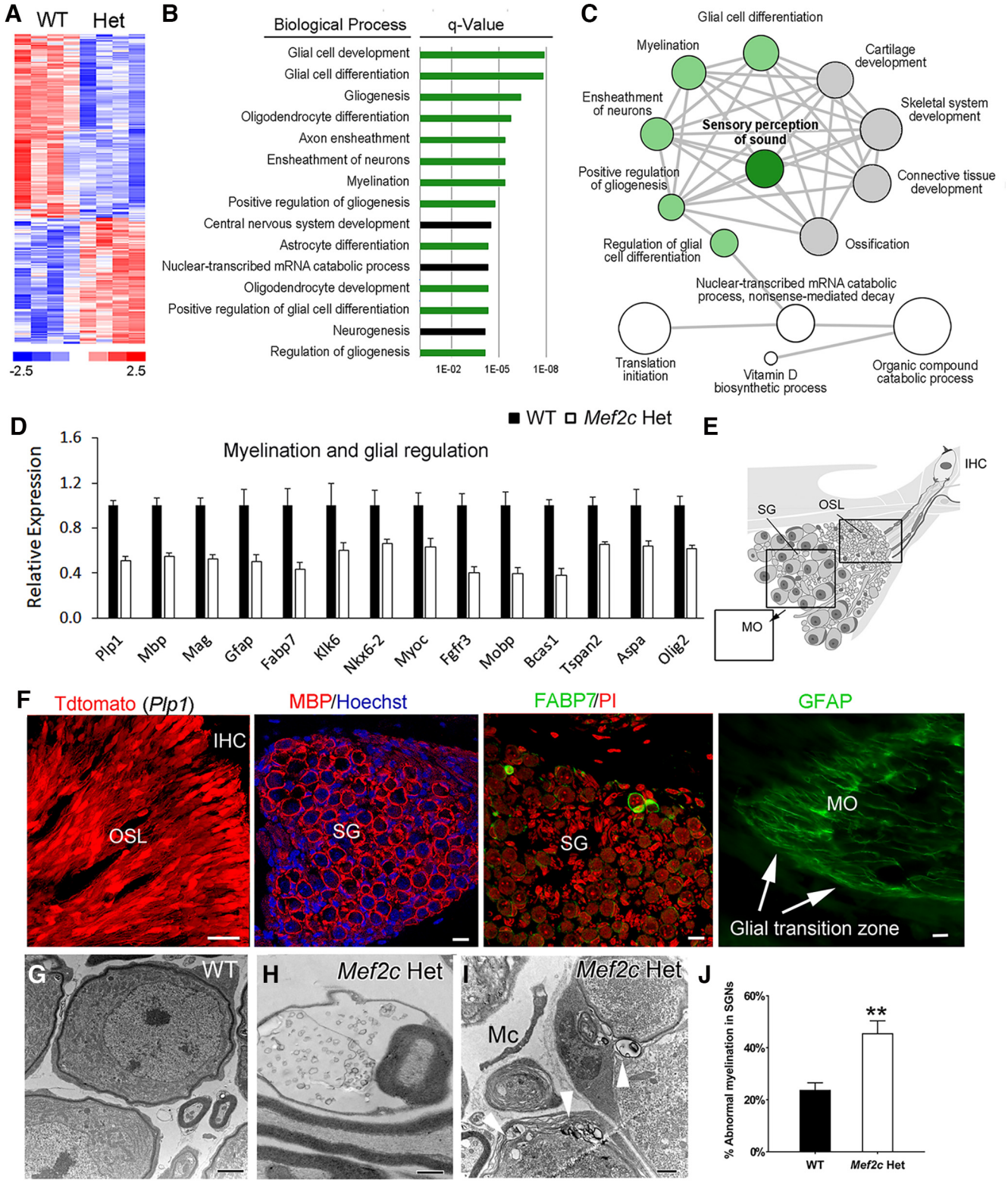

Figure 4. Gene expression alterations related to glial cell function and abnormal myelination in the AN of *Mef2c*-Het mice. ***A***, RNA-seq analysis identified 258 genes differentially expressed in AN of *Mef2c*-Het mice (Extended Data Fig. 4-1). Differential expression was defined as absolute fold change >1.5 and *p*adj (FDR step-up) <0.05 between P21 WT and *Mef2c*-Het mice ($n = 4$ samples per group; 4 AN collected from 2 mice per sample). ***B***, Biological process enrichment results for differentially expressed genes shown in ***A***. Significant gene terms and scores (Benjamini–Hochberg-adjusted $p < 0.05$) are shown. ***C***, Interactive graph of enriched biological process terms summarized with REVIGO (Supek et al., 2011). ***C*** Node size reflects the number of differentially expressed genes; colored nodes (green or gray) represent the central grouping of highly similar categories relating to sensory perception of sound. ***B***, ***C***, Green represents biological processes relating to glial cells. ***D***, Downregulation of genes related to myelination and glial regulation. ***E***, Schematic image of AN cross-section illustrating areas along AN within OSL, spiral ganglion (SG) in Rosenthal's canal, and modiolus (MO). ***F***, Immunohistochemical detection in mouse ANs for the glial cell markers that were found to be downregulated by RNA-seq. Shown are Schwan cells within OSL (*Plp1*), satellite cells around Type I SGNs (MBP), satellite cells around Type II SGNs (FABP7), and glial cells in the AN central process (GFAP; arrows) in MO. ***G***, EM graph represents healthy appearance of the SGNs in young adult WT animals. ***H–J***, Disruption of the myelin sheath surrounding an axon (***H***) and SGNs (white arrowheads; ***I***). Percentage of SGNs with abnormal myelin sheaths was greatly increased in *Mef2c*-Het mice (Mann–Whitney *U* test, $p = 0.0043$, $n = 4$ mice/group; ***J***). Scale bars: ***F***, 10 μm; ***G***, 2 μm; ***H***, ***I***, 1 μm.

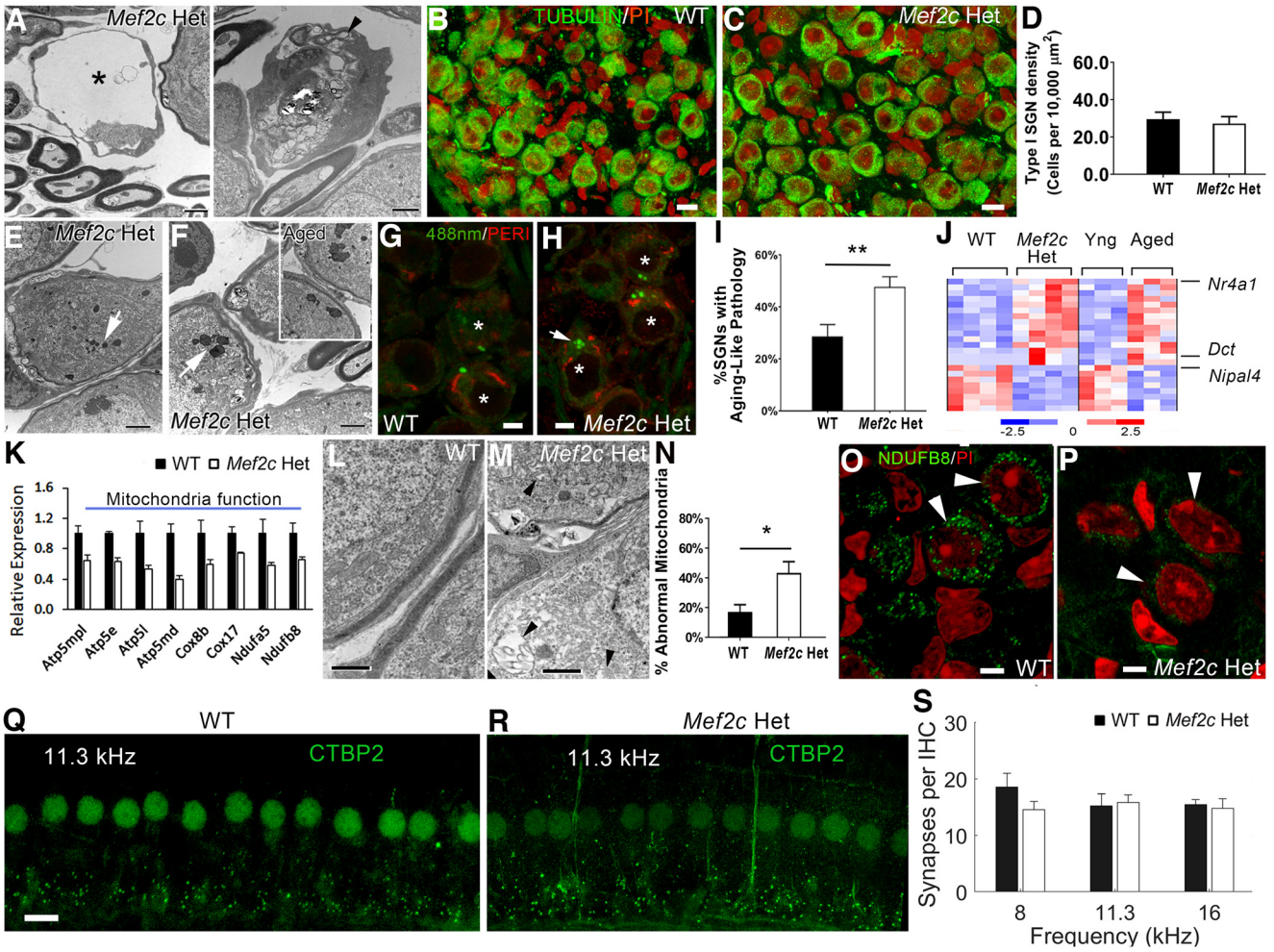

Figure 5. Aging-like neuronal changes and mitochondrial dysfunction in the ANs of *Mef2c*-Het mice. ***A***, ***B***, Degenerative SGNs (*; an arrowhead) were seen in EM graphs of young adult *Mef2c*-Het mice. ***B–D***, No significant loss of SGNs was identified in young adult *Mef2c*-Het mice ($p > 0.05$, Mann–Whitney *U* test; $n = 3$ animals per group). Type I SGNs of young adult WT and *Mef2c*-Het mice were stained with anti-β III-tubulin (β-Tubulin; green) antibody. Nuclei were stained with propidium iodide (PI). ***E***, ***F***, ***I***, Increased aging-like pigment (white arrows in ***E***, ***F***) were seen in SGNs of young adult *Mef2c*-Het mice ($p = 0.004$, Mann–Whitney *U* test; $n = 4$ animals per group). ***F***, Right, The aging pigment in SGNs of aged CBA/CaJ mice aged 2.5 years. ***G***, ***H***, Aging pigment is detected by autofluorescence. Aging pigment (a arrow) was often seen in Type I SGN soma that contained low-intensity peripherin (PERI) labeled intermediate neurofilaments (red), but was not seen in areas in which nuclei were located (*). ***J***, Evaluation of RNA-seq data found that 23 genes differentially expressed in *Mef2c*-Het AN also changed in aging AN (gene list is included in Extended Data Fig. 5-1). ***K***, Mitochondrial function genes downregulated in *Mef2c*-Het AN. ***L–P***, *Mef2c*-Het mice mitochondrial abnormalities in AN. ***L***, ***M*** TEM of young adult AN in WT and *Mef2c*-Het. ***M***, Black arrowheads indicate abnormal mitochondria in SGNs. ***N***, *Mef2c*-Het mice display an increased number of abnormal mitochondria ($p = 0.029$, Mann–Whitney *U* test, $n = 3$ animals per group). ***O***, ***P***, Altered distribution of the mitochondrial regulator NDUFB8 (arrowheads) in SGN of *Mef2c*-Het AN. ***Q-S***, Number of ribbon synapses of Type I SGNs in young adult *Mef2c*-Het mice appeared normal. Ribbon synapses, a subset of AN fibers and IHC nuclei were stained positively with anti-CTBP2 antibody. No significant change in $CTBP2^+$ synapse number was seen in the 8, 11.3, and 16 kHz frequency areas of the *Mef2c*-Het mice ($n = 4$ or 5) compared with WTs ($n = 3$-5) (Type III ANOVA; $p = 0.383$, 0.705, and 0.406 for main effects of genotype, frequency, and the interaction of genotype × frequency, respectively). Scale bars: ***A***, ***E***, ***F***, 2 μm; ***B***, ***C***, ***Q***, 10 μm; ***G***, ***H***, ***O***, ***P***, 5 μm; ***L***, ***M***, 1 μm.

may be a small fraction of the total. Consistent with these findings, counts of $CTBP2^+$ synapses of Type I SGNs revealed no significant difference in the synapse numbers at the apical-middle portion of the cochlear duct (Fig. 5*Q–T*).

One of the striking hallmarks in aging neuronal cells is the accumulation of lipofuscin granules or neuromelanin pigments (also named "aging pigments") in the cellular compartment of the soma as shown in SGNs of an aged CBA/CaJ mouse (Fig. 5*F*, left) (Riga et al., 2006; Sulzer et al., 2008; Jung et al., 2010). Interestingly, aging-like SGNs were more often seen in young adult *Mef2c*-Het mice than their WT littermate controls (Fig. 5*E*, *F*, right). As shown in Figure 5*I*, quantitative analysis of EM graphs from middle turns of young adult mice revealed that 47 ± 4% of SGNs in *Mef2c*-Het mice had at least two lipofuscin granules while only 29 ± 5% of SGNs in WT had this aging-like characteristic. The increase in these lipofuscin (or neuromelanin) inclusions was also validated by fluorescence microscopic detection of the autofluorescent inclusions (Fig. 5*G*,*H*) (Jung et al., 2010). To further evaluate the premature aging-like phenomenon in young adult *Mef2c*-Het mice SGNs, we examined expression profiles of DEGs obtained from our RNA-seq analysis of *Mef2c*-Het AN using a prior RNA-seq dataset that tested the effect of aging (Panganiban et al., 2022). Our analysis found that 23 of the genes affected in *Mef2c*-Het AN were also significantly affected (p adj < 0.1) in aging AN and agreed in direction of change (Fig. 5*J*; Extended Data Fig. 5-1). Dopachrome tautomerase (*Dct*) is a Type I membrane protein and a key regulator of biosynthesis of melanin, including neuromelanin, which can form a similar type of pigment accumulation in aging nervous tissue (Costin et al., 2005; Double et al., 2008). Nipa-like domain-containing 4 (*Nipal4*) is involved in synthesis of long-chain fatty acids and plays a role in lipid metabolism (Dahlqvist et al., 2012).

Nuclear receptor 4A1 (*Nr4a1*) is a mediator of macrophage function and plays a role in regulating inflammatory responses. Translocation of Nr4a1 protein from the nucleus to mitochondria leads to apoptosis (Bouzas-Rodríguez et al., 2012). Together, combined quantitative ultrastructural evaluation and RNA-seq analysis revealed subcellular and molecular evidence of AN dysfunction in young adult *Mef2c*-Het mice.

Ultrastructural examination of young adult mouse AN found that there were pathologic alterations in some mitochondria and that these alterations were more frequently seen in *Mef2c*-Het animals (Fig. 5*L–N*). Alterations included increased intraorganelle space and separation of cristae. A count of healthy and pathologic mitochondria was completed on randomly selected axon EM graphs that were taken from the middle portions of cochlea from WT and *Mef2c*-Het mice. Our data revealed a significant increase in abnormal mitochondria in the *Mef2c*-Het mice; ~43% of examined mitochondria were abnormal in *Mef2c*-Het mice ($n = 4$), whereas only 17% of examined mitochondria were abnormal in WT controls. To further validate these results, a reexamination of RNA-seq data for the 258 DEGs affected in *Mef2c*-Het AN found that eight genes were related to mitochondria function and all were downregulated (Fig. 5*K*). Immunohistochemical analysis for one of these, NADH dehydrogenase [ubiquinone] 1 β subcomplex/subunit 8 (NDUFB8), found that expression of Ndufb8 was high in mitochondria of SGNs in WT mice, but it was weak in SGN of *Mef2c*-Het mice (Fig. 5*K*,*O*,*P*). Again, quantitative ultrastructural evaluation and gene expression analysis revealed that mitochondrial dysfunction may be one mechanism underlying AN functional decline in the *Mef2c*-Het mice.

Mef2c-Het mice exhibit increased inflammation and macrophage activation in AN and stria vascularis

Our previous study showed that Mef2c hypofunction in microglia leads to dysregulation of microglial genes and ASD-related behaviors (Harrington et al., 2020). Based on those findings, we hypothesized that Mef2c deficiency would cause abnormal macrophage activity in the AN and its surrounding cochlear environment (e.g., cochlear vasculature in the AN and stria vascularis). Cochlear ultrastructural examination (Fig. 6*A–D*,*F*,*G*), gene expression analysis of AN (Fig. 6*E*), and immunohistochemical evaluation of AN macrophages and microvasculature (Fig. 6*H*) and stria

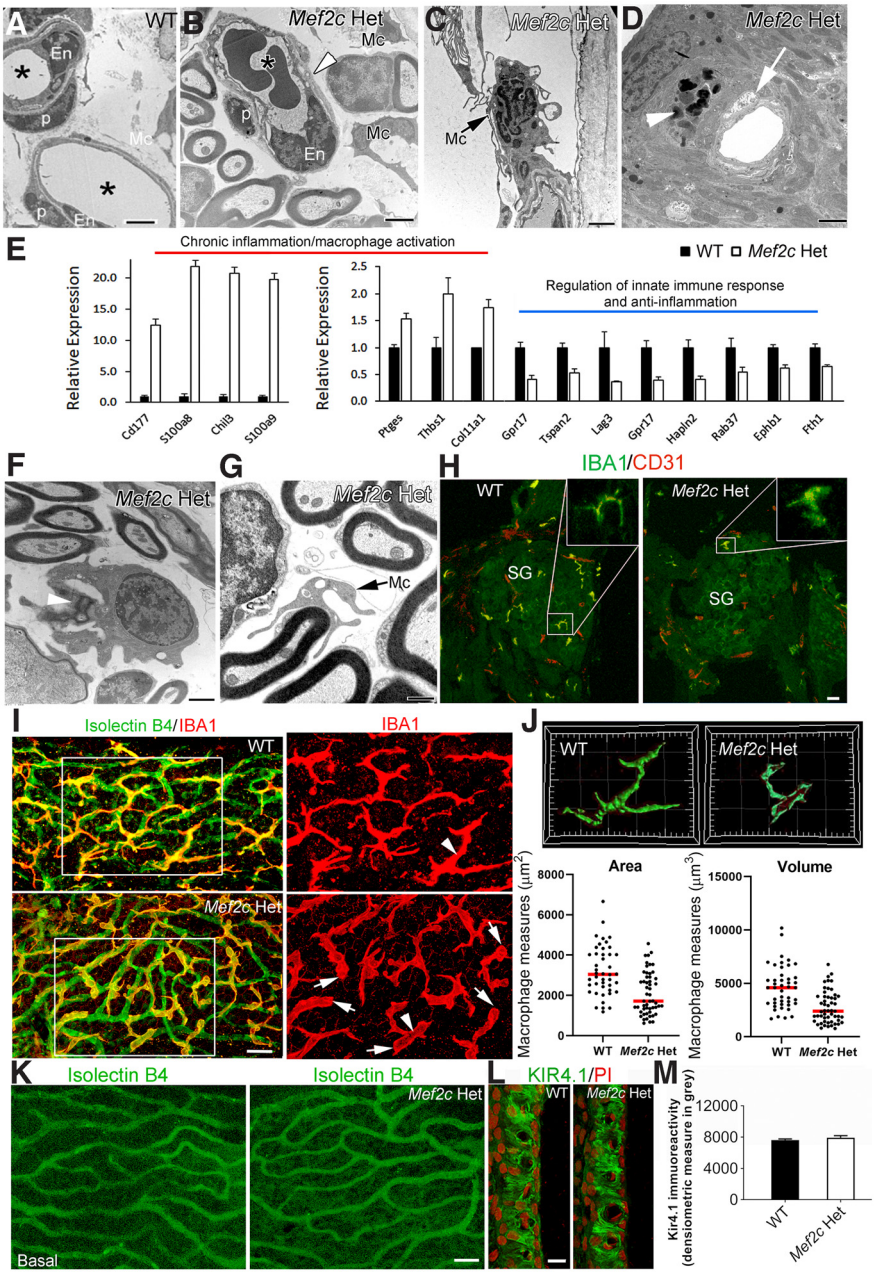

Figure 6. Mef2c deficiency causes an increased cochlear inflammation and macrophage activation in AN and stria vascularis of young adult mice. ***A-D***, EM graphs show pathologic alteration in microvasculature (white arrowhead in ***B***; white arrow in ***D***), frequently engaging with activated macrophage (Mc, black arrow in ***C***), in *Mef2c*-Het AN (***B***,***C***), and stria vascularis (***D***). TEM graph in ***A*** shows endothelial cells (En) adjacent to pericytes (p) in a normal-appearing microvasculature in AN. Asterisks indicate capillary lumens. ***D***, White arrowhead indicates a perivascular macrophage-like melanocyte (characterization based on previous studies by Zhang et al., 2012) located around the disrupted microvasculature in stria vascularis of a *Mef2c*-Het mouse. ***E***, Changes in expression of genes related to chronic inflammation/macrophage activation, regulation of innate immune response, and anti-inflammation. ***F***, ***G***, TEM graphs show a macrophage cell engulfing myelin debris (***F***) and a macrophage process surrounding a healthy axon (***G***). ***H–M***, Increase in macrophages with activated morphology and changes in interaction between macrophages and microvasculature in AN and stria vascularis of young adult *Mef2c*-Het mice. CD31 antibody (***H***) or isolectin GS-IB4 (isolectin-B4) conjugated with AlexaFluor (***I***) were used for labeling microvasculature. IBA1 antibody was used as a marker for identifying macrophages. Bottom, 3D views of selected macrophages in ***I*** (white arrowheads) generated with the Surface module of IMARIS (IMARISx64 9.3.1). Quantitative analysis of macrophage morphology reveals reduced surface area and cellular volume in the stria vascularis of young adult *Mef2c*-Het mice (***J***, bottom; 44 and 53 macrophages were randomly selected and measured from 3 WTs and 3 Hets, respectively. For detailed statistical analysis information, see Extended Data Figure 6-1. Although there is increased macrophage activity, no remarkable change in isolectin-B4$^+$ microvasculature was identified in the stria vascularis of young adult *Mef2c*-Het mice (***I***,***K***). No significant change in KIR4.1 immunoactivity was identified in the strial vascularis of young adult *Mef2c*-Het animals compared with that of WTs ($p = 0.3$, Mann–Whitney *U* test; $n = 3$ for WT and $n = 4$ for *Mef2c* Het) (***L***,***M***). Scale bars: ***A–D***, ***F***, 2 μm; ***G***, 800 nm; ***H***, ***L***, 15 μm; ***I***, ***K***, 20 μm.

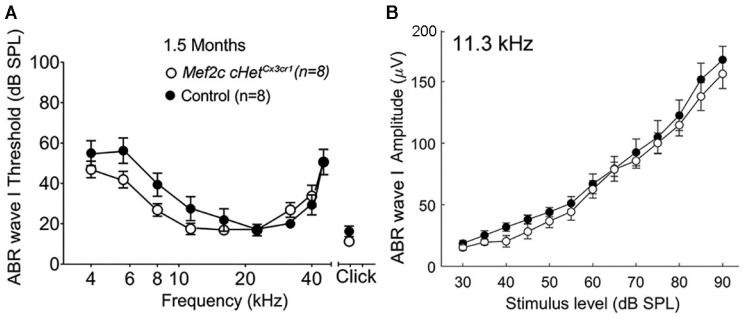

Figure 7. No significant changes of auditory function in *Mef2c cHet*^{Cx3cr1} mice. ***A***, The averaged ABR wave I thresholds are shown in young adult WTs and *Mef2c cHet*^{Cx3cr1} mice. No significant threshold shifts were seen in *Mef2c cHet*^{Cx3cr1} animals compared with littermate controls (for detailed statistical analysis information, see Extended Data Fig. 7-1). ***B***, No significant change was seen in ABR wave I amplitude I/O functions at 11.3 kHz between WTs and *Mef2c cHet*^{Cx3cr1} mice (Extended Data Fig. 7-1).

vascularis (Fig. 6*I*,*J*) all yielded results that support this hypothesis. First, microvasculature was disrupted in young adult *Mef2c*-Het AN (Fig. 6*B*,*C*) and stria vascularis (Fig. 6*D*), and macrophages can be seen interacting with the abnormal vasculature. Second, RNA-seq findings showed upregulation of genes relating to chronic inflammation and macrophage activation, but downregulation of genes involved with innate immune response and anti-inflammation in *Mef2c*-Het AN (Fig. 6*E*), including *S100a8, S100a9, Chil3*, and *Cd177*. Qualitative and quantitative morphometric analysis further showed that macrophage activation was increased (Fig. 6*F–J*) (Extended Data Fig. 6-1) and macrophage and microvasculature interactions affected in *Mef2c*-Het mice (Fig. 6*I*). TEM revealed interactions between macrophages and neurons and the uptake of myelin debris through phagocytosis (Fig. 6*F*). The presence of myelin-filled lysosomes within macrophages is suggestive of demyelination and neuron degeneration, as previously observed in a noise-induced AN degeneration model (Panganiban et al., 2018). Immunohistochemistry performed on 20-μm-thick AN sections and whole-mount preparations of stria vascularis show that there was an increase in the number of macrophages with activated morphology, especially in the apical turn, based on retracted processes and reduced cellular area and volume (Fig. 6*H–J*; $p < 0.0001$; for both cellular area and volume measure, unpaired, two-tailed *t* test with Welch's correction). To further test the impact of MEF2C deficiency on the strial function, we quantitatively evaluated the immunoactivity of inwardly rectifying potassium channel 4.1 (KIR4.1) (Fig. 6*L*,*M*). KIR 4.1 is expressed in intermediate cells and plays an important role in the maintenance of the high K^+ concentration and generation of the endocochlear potential (Liu et al., 2019). In agreement with the KIR immunostaining results, no remarkable loss of the strial capillaries was identified by the isoclactin B4 staining approach (Meyer et al., 2008) (Fig. 6*I*,*K*). Our data revealed there are no significant changes in the intermediate cells and strial capillary in *Mef2c* Hets compared with that of WTs, suggesting a limited impact of MEF2C deficiency in cochlear lateral wall functioning.

To further test the hypothesis that Mef2c deficiency in immune cells (e.g., Cx3cr1-expressing cochlear macrophage) leads to cochlear pathology and AN functional decline, young adult *Mef2c*$^{flox/+}$*; Cx3cr1-Cre* mice were examined for ABR wave I threshold and suprathreshold function. As shown in Figure 7, there were no significant alterations in wave I ABR threshold or suprathreshold function in *Mef2c*$^{flox/+}$*; Cx3cr1-Cre* mice compared with that of their littermate controls (Extended Data Fig. 7-1), suggesting that deficiency of Mef2c in immune cells alone may not lead to AN functional decline.

Mef2c deficiency has no gross effect on HC function and cochlear bone formation

Since *Mef2c*-Het mice showed a significant reduction of ABR wave I threshold in low- and middle-frequency ranges compared with controls, we examined whether there were functional declines or pathologic alterations in sensory HCs. Functional and structural analyses of sensory HCs in *Mef2c*-Het mice did not detect an overt effect on sensory HCs (Fig. 8). That was supported by CM measurement, which detected no significant difference between the young adult WTs and *Mef2c*-Het mice (Fig. 8*A*; Extended Data Fig. 8-1), suggesting no significant loss of OHC function in *Mef2c*-Het mice. Furthermore, histologic analysis did not reveal gross morphologic changes in apical and middle portion cochlear structure, using either cochlear sections (Fig. 8*B*) or whole-mount preparations (Fig. 8*C–F*). Since MEF2C protein was detected in bone forming cells around the cochlear duct (Fig. 1*H*,*K–M*), we next examined whether MEF2C deficiency affected bone formationin the ossicles and cochlear bony capsule. As shown in Figure 8*G–I*, no gross changes were evident in the cochlear bony capsule (Fig. 8*G*), ossicles (Fig. 8*H*), or bone structure around the AN (Fig. 8*I*), suggesting that MEF2C deficiency was not sufficienct to disrupt middle and innea ear bone formation.

Discussion

Establishment of animal models of human ASD with well-characterized AN functional deficiency is a crucial first step toward understanding the contribution of peripheral AN dysfunction to communication deficits and other ASD behaviors. However, to date, only a small number of auditory investigations have been done with ASD animal models. Among those studies, peripheral AN functional decline was well characterized in a mouse model of Fragile X syndrome (*Fmr*1 KO mice) (Rotschafer et al., 2015). ABR wave I amplitude growth function measures in *Fmr1*$^{-/-}$ mice suggested a decline in peripheral AN activity, together with an ~10 dB SPL threshold elevation and deficits in auditory brainstem function. Previous studies also showed that mouse and rat models of Fragile X syndrome exhibit hypersensitivity and auditory processing dysfunction (Rotschafer and Razak, 2013; Garcia-Pino et al., 2017; El-Hassar et al., 2019; McCullagh et al., 2020; Auerbach et al., 2021). In addition, abnormal ABRs were reported in *Adnp* haploinsufficient (*Adnp*$^{+/-}$) mice, another animal model of ASD-linked gene deficiency (Hacohen-Kleiman et al., 2019). Those studies revealed that ASD models exhibited auditory impairment but provided only limited information regarding possible changes in peripheral auditory organ or pathologic alterations of AN degeneration and dysfunction, which is critical for understanding the link between AN function and ASD characteristics, such as sensory hypersensitivity and social communication deficits. Here we report that a model of human MEF2C hypofunction with well-defined ASD-like behaviors (Harrington et al., 2020) has a modest reduction in hearing sensitivity combined with AN functional deficits. This study is significant in that it: (1) links a monogenic ASD animal model with a clear impairment in peripheral AN structure and function,

and (2) reveals a critical new role for Mef2c function in normal peripheral AN development and function.

Functional and structural integrity of the peripheral AN is critical for proper auditory processing in the central auditory system. However, ABR wave I threshold only represents the function of the most sensitive AN fibers; therefore, threshold is not regarded as a sensitive approach for assessing AN integrity. For example, a well-established mouse model of noise-induced hearing loss showed robust primary AN degeneration, but only a limited change in the threshold of ABR wave I (or the AN compound action potential threshold) (Kujawa and Liberman, 2009; Liberman, 2017). Measures of AN threshold are dependent on a small subset of AN fibers with high SR and low thresholds. In contrast, suprathreshold measures of AN function may reflect the contribution of AN fibers with varied SR and thresholds depending on level and stimulus parameters of the eliciting stimulus. Combining *in vivo* noninvasive measurement of AN synchrony by PLV together with ABR wave I amplitude growth functions (AN suprathreshold measures), our study found that *Mef2c*-Het mice have suprathreshold peripheral AN functional decline. For example, at 11.3 kHz, the frequency showing AN functional decline, the elevated thresholds were <9 dB SPL, with no significant threshold shifts in the higher frequencies. These results agree with previous findings that there was no association between hearing loss and human MCHS, although difficulty with speech, intellectual disabilities, seizures, stereotypic movements, vision issues, and other ASD-like behaviors were well documented in MCHS patients (Cooley Coleman et al., 2021). While there remains only limited evidence in humans that AN dysfunction is linked to ASD (Santos et al., 2017), peripheral AN deficits are known to contribute to changes in higher levels of the central auditory system, including sensory hypersensitivity and auditory processing dysfunction. Our recent studies reported that poorer PLV in humans with otherwise normal audiograms is associated with poorer auditory processing and speech recognition (Harris et al., 2018, 2021). Together, results of the current study highlight the potential clinical utility of suprathreshold peripheral AN functional evaluation as one potential diagnostic indicator of ASD. This technique was first developed and tested in human subjects, data can be acquired without active subject participation, and the procedure is relatively noninvasive (Harris et al., 2018, 2021).

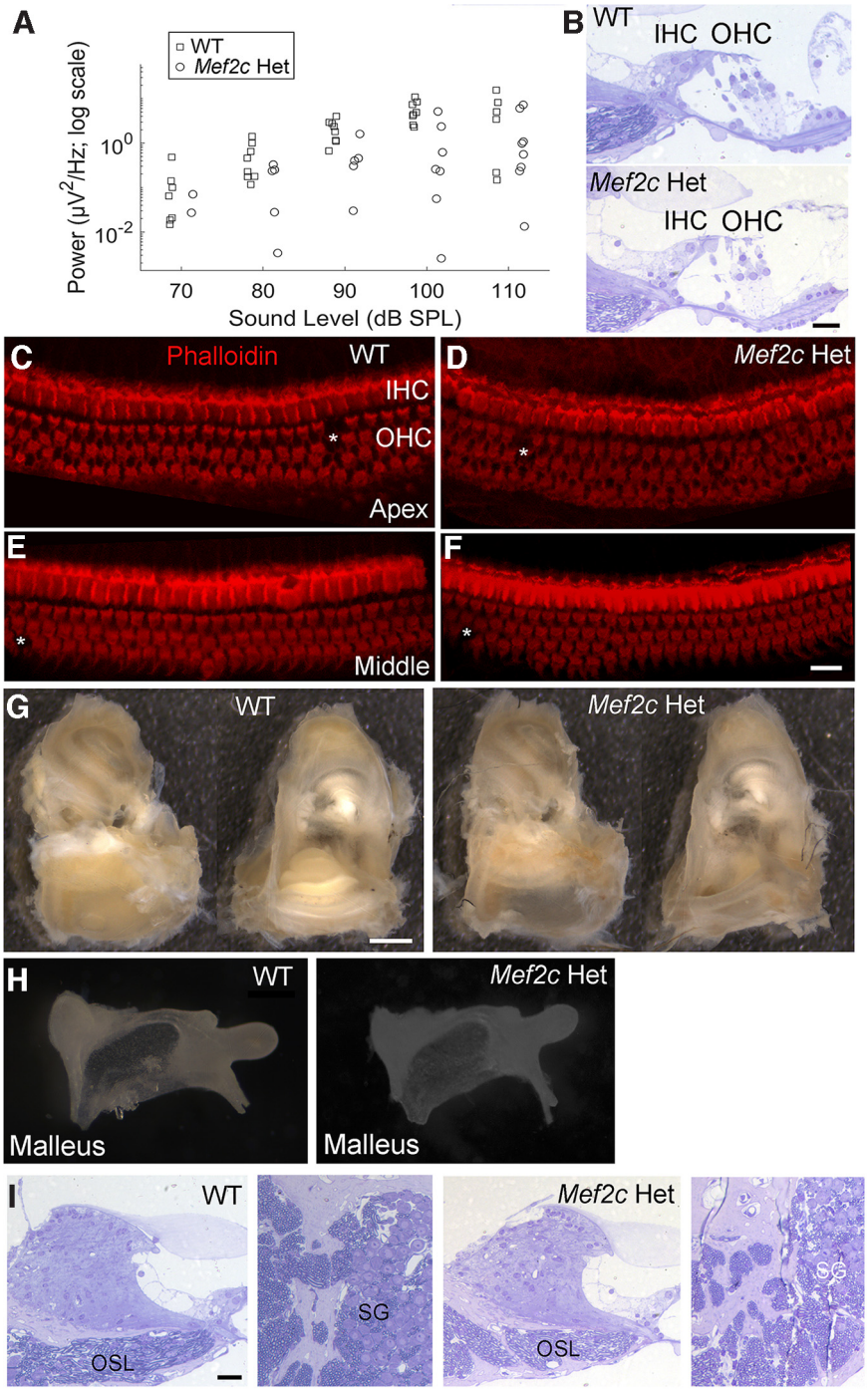

Figure 8. Evaluation of sensory HCs, ossicles, and cochlear bony capsules in young adult *Mef2c*-Het mice. ***A***, No difference in CM response was identified between young adult WT and *Mef2c*-Het mice (for detailed statistical analysis information, see Extended Data Fig. 8-1). ***B***, Representative images of toluidine blue-stained organs of Corti from the middle portion of the cochlea showing IHCs and OHCs in young adult WT and *Mef2c*-Het mice. ***C–F***, Surface preparations from apical (***C***,***E***) and middle (***D***,***F***) portions of cochlea from WT (***C***,***E***) and *Mef2c*-Het (***D***,***F***) cochleae. Very infrequent HC loss (*) was seen in both groups. ***G***, ***H***, No significant change was observed in the bony inner ear portion of temporal bones (***G***; left, side view of cochlea; right, view from the internal auditory canal) or ossicles (***H***) of young adult *Mef2c*-Het mice. ***I***, Representative images of toluidine blue-stained AN from the middle portion of young adult WT and *Mef2c*-Het mice showing the bony structures around OSL and SG. Scale bars: ***B–F***, ***I***, 20 μm; ***G***, 600 μm.

Another important finding of this study is that the *Mef2c*-Het mice exhibit multiple cellular and molecular alterations that likely contribute to the peripheral AN functional decline. These alterations included glial cell dysfunction and myelin abnormality, aging-like SGN degeneration (e.g., lipofuscin and/or neuromelanin accumulation), neuronal mitochondrial dysfunction, and increased macrophage activation

and inflammation. A microdeletion or point mutation within the protein-coding region of the *MEF2C* gene on chromosome 5 results in reduced MEF2C protein levels and function is one established cause of human MCHS (Le Meur et al., 2010; Mikhail et al., 2011; Tonk et al., 2011). Brain MRI studies in MCHS patients suggested that MEF2C mutation is also associated with delayed neuron myelination (Zweier et al., 2010; Rocha et al., 2016). In agreement with this observation, our analysis of *Mef2c*-Het RNA-seq and ultrastructural data supports the finding of glia dysfunction and abnormal myelination. It is generally accepted that the amplitude and synchrony of AN activity are primarily dependent on the initiation of action potential at the axon initial segment (AIS, or spike initiation zone), a heminode at the habenula opening under IHCs (Hossain et al., 2005). This initial event is trigged by the release of neural transmitters by synapses between IHCs and AN. The disruption across the AIS and downstream structures of the AIS along the AN axon as a result of glial cell dysfunction (e.g., abnormality of the glia-neuron interaction at the heminode and node of Ranvier, and changes in myelin thickness or g ratio) should have a significant impact on the speed and synchrony of nerve activity. A computational model suggested that the length of the node of Ranvier could determine the velocity of axon conduction in the optic nerve and cerebral cortical axon of rats (Arancibia-Cárcamo et al., 2017). Our recent study reported that the length of nodes of Ranvier along the axon is associated with neural processing speed and synchrony in the AN (Panganiban et al., 2022). This study also showed that stimulus level-dependent amplitude growth is associated with nodes of Ranvier that are located closely around neuron soma of the AN. Together, this evidence supports that MEF2C deficiency associated glial dysfunction may be an important contributor to the AN function declines (e.g., a weakened synchrony and reduced amplitude of ABR wave I response) seen in this syndromic ASD model.

Interestingly, while MEF2C was found to be present in many different cell types within adult AN, it was not found in mature glial cells (Fig. 1). This suggests that the observed consequences on glial cell gene expression and myelination are not because of MEF2C function within mature glia but may be the result of signaling from other cell types or as a secondary response to SGN dysfunction and/or increased cochlear inflammation and macrophage activation. Bioinformatic analysis of genes identified as ASD-related and AN developmentally regulated found that 18 were also putative MEF2C targets in microglia (Deczkowska et al., 2017; Bjorness et al., 2020). Interestingly, the molecular function "signaling receptor binding" was among the most enriched category for these genes, suggesting the potential for MEF2C to elicit an effect on glia through a neuron-to-glia signaling mechanism. Notable among the genes was acetylcholinesterase, which is a chemical transmitter that regulates neuron-glial crosstalk and neuropathic pain in sensory ganglion (Matsuka et al., 2020).

Although no significant neuronal cell loss was found in *Mef2c*-Het mice, AN functional decline was supported by aging-like SGN degeneration, including neuronal mitochondrial dysfunction. Previous studies revealed that MEF2 family members regulate transcription of both the nuclear and mitochondrial genomes and that their inhibition can cause decreased activity of mitochondrial complex I (ubiquinone oxidoreductase), increased hydrogen peroxidase levels, and reduced ATP production (Naya et al., 2002; She et al., 2011). In skeletal muscle, MEF2C plays a role in regulating metabolic homeostasis and affects animal body size (Anderson et al., 2015). The importance of the link between MEF2 and mitochondrial function was also highlighted in investigations of neuronal structural and functional plasticity (Brusco and Haas, 2015). In the AN of young adult *Mef2c*-Het mice, our RNA-seq analysis detected downregulation of several mitochondrial genes, including mitochondrial complex I protein NDUFB8. Distribution of NDUFB8 protein was also found to be affected in neuronal soma of *Mef2c*-Het AN. Together with the observed disruption of mitochondrial structure, the dysregulation of mitochondrial genes related to complex I activity suggests that mitochondrial hypofunction may be a cause of AN functional decline in *Mef2c*-Het mice. Previous studies showed that reduced mitochondrial complex I activity contributes to mitophagy dysfunction, which results in an increased number of damaged mitochondria in neuronal cells in neurodegenerative diseases (Franco-Iborra, et al., 2018). Accumulation of damaged mitochondria and autophagic vacuoles filled with lipofuscin or neuromelanin pigments is a hallmark of age-related neurodegeneration and is also associated with neuronal loss (Sulzer et al., 2008; Moreno-García et al., 2018; Fang et al., 2019). Previous studies also suggest that an interaction between senescent lipofuscin and mitochondria may play a role in progression of cellular degeneration (Terman et al., 2007; König et al., 2017). Based on these observations, we hypothesize that *Mef2c* hypofunction contributes to aging-like mouse AN degeneration via a negative impact on mitochondrial function and cellular metabolism.

Transcriptomic analysis of postmortem brain tissues from individuals with autism has revealed expression changes in microglial-specific genes and genes related to inflammatory response (Voineagu et al., 2011; Gupta et al., 2014; Velmeshev et al., 2019). Recent studies revealed that MEF2C expression in microglia/macrophages is also important for brain development and maintenance of cognitive function in adults (Deczkowska et al., 2017; Harrington et al., 2020). Here our study revealed that MEF2C is expressed in neurons as well as in microglia/macrophages in the AN of the peripheral auditory system. In the peripheral auditory system, we found that *Mef2c*-Het mice demonstrated an increase in macrophage activation in the AN and the stria vascularis, an increase in mRNA expression of pro-inflammatory genes, and morphologic disruption of microvasculature. There are at least three factors that may lead to increased IBA1 expressing cells in the cochlea: (1) as a direct result of Mef2c deficiency (since MEF2C is highly expressed in $IBA1^{+}$ cochlear macrophage); (2) as a result of dysfunction of the SGN; and (3) a consequence of the degeneration of glial cells in the AN. Our data showing increased inflammatory cells in the strial vascularis also suggest the direct impact of Mef2c deficiency in cochlear macrophages in multiple cochlear locations. Although the current study did not establish whether increased macrophage activation was a direct result of *Mef2c* hypofunction in those cells, SGN aging-like degeneration, or both, our data clearly reveal that the AN functional decline is accompanied by increased macrophage activation and a shift in the cochlea toward pro-inflammatory status.

Conditional deletion of one copy of *Mef2c* in *Cx3Cr1*-expressing cells (macrophages and other immune cell subtypes) in mice [$Mef2c^{flox/+}$; *Cx3cr1-Cre* (*Mef2c* $cHet^{Cx3cr1}$) mice] resulted in social interaction deficits and increased repetitive behavior (Harrington et al., 2020), suggesting that *MEF2C* haploinsufficiency in neuroimmune cells may produce ASD-related behaviors. However, in the peripheral auditory system, no significant alterations in auditory function were observed in the *Mef2c* $cHet^{Cx3cr1}$ mice, suggesting that a partial deletion of *Mef2c* in cochlear macrophages alone may not be enough

to cause AN functional declines. Further study is needed to address the specific mechanistic relationships and whether inhibition of macrophage activation is a potential treatment strategy for improving AN function and reducing other ASD-related communication impairments.

Finally, our study provides a paradigm for evaluating AN functional decline at the physiological, cellular, and molecular levels in mouse models with only minimal hearing threshold changes. Comprehensive structural and functional characterization of the peripheral AN is a critical step in evaluating the relationship between peripheral auditory function and sensory hypersensitivity and other auditory processing impairments, whether in ASD or other common neurodevelopmental and neurodegenerative disorders. Measurement of ABR threshold and standard histologic evaluation, such as SGN counting, are not sensitive approaches for identifying AN functional decline with mild or no hearing threshold elevation (termed "hidden hearing loss"). Taking advantage of high-resolution imaging technology, the establishment of cochlear synaptopathy (loss of synaptic connections between AN fibers and cochlear HCs) demonstrates the importance of primary AN degeneration in several forms of sensorineural hearing loss (Liberman, 2017; Liberman and Kujawa, 2017). The paradigm presented here combines comprehensive AN physiology (including intertrial coherence) with high-resolution imaging of non-neuronal cells and transcriptomic analysis for evaluating the functional state of the peripheral AN. Using a model that displays a mild level of hearing loss, the application of this approach was able to detect deficiency in several non-neuronal elements, including glial cell dysfunction, myelination abnormality, alteration in cochlear microvasculature, and elevated macrophage activation that may directly or indirectly contribute to AN functional declines and degeneration.

References

Amaral D, Schumann C, Nordahl C (2008) Neuroanatomy of autism. Trends Neurosci 31:137–145.

Anderson CM, Hu J, Barnes RM, Heidt AB, Cornelissen I, Black BL (2015) Myocyte enhancer factor 2C function in skeletal muscle is required for normal growth and glucose metabolism in mice. Skelet Muscle 5:7– 7.

Amir I, Lamerton D, Montague M (2018) Hyperacusis in children: the Edinburgh experience. Int J Pediatr Otorhinolaryngol 112:39–44.

Arancibia-Cárcamo IL, Ford MC, Cossell L, Ishida K, Tohyama K, Attwell D (2017) Node of Ranvier length as a potential regulator of myelinated axon conduction speed. Elife 6:7e23329.

Auerbach BD, Manohar S, Radziwon K, Salvi R (2021) Auditory hypersensitivity and processing deficits in a rat model of fragile X syndrome. Neurobiol Dis 161:105–541.

Bates D, Mächler M, Bolker B, Walker S (2015) Fitting linear mixed-effects models using lme4. J Stat Softw 67:1–48.

Bennetto L, Keith J, Allen P, Luebke A (2017) Children with autism spectrum disorder have reduced otoacoustic emissions at the 1 kHz mid-frequency region. Autism Res 10:337–345.

Bjorness TE, Kulkarni A, Rybalchenko V, Suzuki A, Bridges C, Harrington AJ, Cowan CW, Takahashi JS, Konopka G, Greene RW (2020) An essential role for MEF2C in the cortical response to loss of sleep in mice. Elife 9:e58331.

Bouzas-Rodríguez J, Zárraga-Granados G, Sánchez-Carbente Mdel R, Rodríguez-Valentín R, Gracida X, Anell-Rendón D, Covarrubias L, Castro-Obregón S (2012) The nuclear receptor NR4A1 induces a form of cell death dependent on autophagy in mammalian cells. PLoS One 7: e46422.

Brown LN, Xing Y, Noble KV, Barth JL, Panganiban CH, Smythe NM, Bridges MC, Zhu J, Lang H (2017) Macrophage-mediated glial cell elimination in the postnatal mouse cochlea. Front Mol Neurosci 10:407.

Brusco J, Haas K (2015) Interactions between mitochondria and the transcription factor myocyte enhancer factor 2 (MEF2) regulate neuronal structural and functional plasticity and metaplasticity. J Physiol 593:3471–3481.

Chambers A, Resnik J, Yuan Y, Whitton J, Edge A, Liberman M, Polley D (2016) Central gain restores auditory processing following near-complete cochlear denervation. Neuron 89:867–879.

Cheatham MA, Naik K, Dallos P (2011) Using the cochlear microphonic as a tool to evaluate cochlear function in mouse models of hearing. J Assoc Res Otolaryngol 12:113–125.

Chen J, Bardes EE, Aronow BJ, Jegga AG (2009) ToppGene Suite for gene list enrichment analysis and candidate gene prioritization. Nucleic Acids Res 37:W305–W311.

Costin GE, Valencia JC, Wakamatsu K, Ito S, Solano F, Milac AL, Vieira WD, Yamaguchi Y, Rouzaud F, Petrescu AJ, Lamoreux ML, Hearing VJ (2005) Mutations in dopachrome tautomerase (Dct) affect eumelanin/pheomelanin synthesis, but do not affect intracellular trafficking of the mutant protein. Biochem J 391:249–259.

Cooley Coleman JA, Sarasua SM, Boccuto L, Moore HW, Skinner SA, DeLuca JM (2021) Comprehensive investigation of the phenotype of MEF2C-related disorders in human patients: a systematic review. Am J Med Genet A 185:3884–3894.

Dahlqvist J, Westermark GT, Vahlquist A, Dahl N (2012) Ichthyin/NIPAL4 localizes to keratins and desmosomes in epidermis and Ichthyin mutations affect epidermal lipid metabolism. Arch Dermatol Res 304:377–386.

de Aguilar-Nascimento JE (2005) Fundamental steps in experimental design for animal studies. Acta Cir Bras 20:2–8.

Deczkowska A, Matcovitch-Natan O, Tsitsou-Kampeli A, Ben-Hamo S, Dvir-Szternfeld R, Spinrad A, Singer O, David E, Winter DR, Smith LK, Kertser A, Baruch K, Rosenzweig N, Terem A, Prinz M, Villeda S, Citri A, Amit I, Schwartz M (2017) Mef2C restrains microglial inflammatory response and is lost in brain ageing in an IFN-I-dependent manner. Nat Commun 8:717.

Delorme A, Makeig S (2004) EEGLAB: an open source toolbox for analysis of single-trial EEG dynamics including independent component analysis. J Neurosci Methods 134:9–21.

Dobin A, Davis CA, Schlesinger F, Drenkow J, Zaleski C, Jha S, Batut P, Chaisson M, Gingeras TR (2013) STAR: ultrafast universal RNA-seq aligner. Bioinformatics 29:15–21.

Do B, Lynch P, Macris E, Smyth B, Stavrinakis S, Quinn S, Constable P (2017) Systematic review and meta-analysis of the association of autism spectrum disorder in visually or hearing impaired children. Ophthalmic Physiologic Optic 37:212–224.

Double KL, Dedov VN, Fedorow H, Kettle E, Halliday GM, Garner B, Brunk UT (2008) The comparative biology of neuromelanin and lipofuscin in the human brain. Cell Mol Life Sci 65:1669–1682.

Edgar J, Khan S, Blaskey L, Chow V, Rey M, Gaetz W, Cannon K, Monroe J, Cornew L, Qasmieh S, Liu S, Welsh J, Levy S, Roberts T (2015) Neuromagnetic oscillations predict evoked-response latency delays and core language deficits in autism spectrum disorders. J Autism Dev Disord 45:395–405.

El-Hassar L, et al. (2019) Modulators of Kv3 potassium channels rescue the auditory function of Fragile X Mice. J Neurosci 39:4797–4813.

Fang EF, Hou Y, Palikaras K, Adriaanse BA, Kerr JS, Yang B, Lautrup S, Hasan-Olive MM, Caponio D, Dan X, Rocktäschel P, Croteau DL, Akbari M, Greig NH, Fladby T, Nilsen H, Cader MZ, Mattson MP, Tavernarakis N, Bohr VA (2019) Mitophagy inhibits amyloid-β and tau pathology and reverses cognitive deficits in models of Alzheimer's disease. Nat Neurosci 22:401–412.

Franco-Iborra S, Cuadros T, Parent A, Romero-Gimenez J, Vila M, Perier C (2018) Defective mitochondrial protein import contributes to complex I-induced mitochondrial dysfunction and neurodegeneration in Parkinson's disease. Cell Death Dis 9:1122.

Garcia-Pino E, Gessele N, Koch U (2017) Enhanced excitatory connectivity and disturbed sound processing in the auditory brainstem of Fragile X mice. J Neurosci 37:7403–7419.

Garreau B, Barthelemy C, Sauvage D, Leddet I, LeLord G (1984) A comparison of autistic syndromes with and without associated neurological problems. J Autism Dev Disord 14:105–111.

Gupta S, Ellis SE, Ashar FN, Moes A, Bader JS, Zhan J, West AB, Arking DE (2014) Transcriptome analysis reveals dysregulation of innate immune response genes and neuronal activity-dependent genes in autism. Nat Commun 5:5748.

Ha S, Sohn IJ, Kim N, Sim H, Cheon K (2015) Characteristics of brains in autism spectrum disorder: structure, function and connectivity across the Lifespan. Exp Neurobiol 24:273–284.

Hacohen-Kleiman G, Yizhar-Barnea O, Touloumi O, Lagoudaki R, Avraham KB, Grigoriadis N, Gozes I (2019) Atypical auditory brainstem response and protein expression aberrations related to ASD and hearing loss in the Adnp haploinsufficient mouse brain. Neurochem Res 44:1494–1507.

Harrington AJ, Raissi A, Rajkovich K, Berto S, Kumar J, Molinaro G, Raduazzo J, Guo Y, Loerwald K, Konopka G, Huber K, Cowan C (2016) MEF2C regulates cortical inhibitory and excitatory synapses and behaviors relevant to neurodevelopmental disorders. Elife 5:e20059.

Harrington AJ, Bridges CM, Berto S, Blankenship K, Cho JY, Assali A, Siemsen BM, Moore HW, Tsvetkov E, Thielking A, Konopka G, Everman DB, Scofield MD, Skinner SA, Cowan CW (2020) MEF2C hypofunction in neuronal and neuroimmune populations produces MEF2C haploinsufficiency syndrome-like behaviors in mice. Biol Psychiatry 88:488–499.

Harris KC, Vaden KI, McClaskey CM, Dias JW, Dubno JR (2018) Complementary metrics of human auditory nerve function derived from compound action potentials. J Neurophysiol 119:1019–1028.

Harris KC, Ahlstrom JB, Dias JW, Kerouac LB, McClaskey CM, Dubno JR, Eckert MA (2021) Neural presbyacusis in humans inferred from age-related differences in auditory nerve function and structure. J Neurosci 41:10293–10304.

Heil P (2004) First-spike latency of auditory neurons revisited. Curr Opin Neurobiol 14:461–467.

Heil P, Irvine DR (1997) First-spike timing of auditory-nerve fibers and comparison with auditory cortex. J Neurophysiol 78:2438–2454.

Helvacioglu F, Dagdeviren A (2019) Myelin ultrastructure terminology in disease and recovery processes. Arch Ital Biol 157:76–88.

Hickox A, Liberman M (2014) Is noise-induced cochlear neuropathy key to the generation of hyperacusis or tinnitus? J Neurophysiol 111:552–564.

Hossain WA, Antic SD, Yang Y, Rasband MN, Morest DK (2005) Where is the spike generator of the cochlear nerve? Voltage-gated sodium channels in the mouse cochlea. J Neurosci 25:6857–6868.

Joubert F, Puff N (2021) Mitochondrial cristae architecture and functions: lessons from minimal model systems. Membranes (Basel) 11:465.

Jung T, Höhn A, Grune T (2010) Lipofuscin: detection and quantification by microscopic techniques. Methods Mol Biol 594:173–193.

Jyothi V, Li M, Kilpatrick LA, Smythe N, LaRue AC, Zhou D, Schulte BA, Schmiedt RA, Lang H (2010) Unmyelinated auditory Type I spiral ganglion neurons in congenic Ly5.1 mice. J Comp Neurol 518:3254–3271.

Kancherla V, Van Naarden Braun K, Yeargin-Allsopp M (2013) Childhood vision impairment, hearing loss and co-occurring autism spectrum disorder. Disabil Health J 6:333–342.

Knipper M, Van Dijk P, Nunes I, Rüttiger L, Zimmermann U (2013) Advances in the neurobiology of hearing disorders: recent developments regarding the basis of tinnitus and hyperacusis. Prog Neurobiol 111:17–33.

Kujawa SG, Liberman MC (2009) Adding insult to injury: cochlear nerve degeneration after 'temporary' noise-induced hearing loss. J Neurosci 29:14077–14085.

König J, Ott C, Hugo M, Jung T, Bulteau AL, Grune T, Höhn A (2017) Mitochondrial contribution to lipofuscin formation. Redox Biol 11:673–681.

Lang H, Nishimoto E, Xing Y, Brown LN, Noble KV, Barth JL, LaRue AC, Ando K, Schulte BA (2016) Contributions of mouse and human hematopoietic cells to remodeling of the adult auditory nerve after neuron loss. Mol Ther 24:2000–2011.

Leifer D, Krainc D, Yu YT, McDermott J, Breitbart RE, Heng J, Neve RL, Kosofsky B, Nadal-Ginard B, Lipton SA (1993) MEF2C, a MADS/MEF2-family transcription factor expressed in a laminar distribution in cerebral cortex. Proc Natl Acad Sci USA 90:1546–1550.

Leifer D, Li YL, Wehr K (1997) Myocyte-specific enhancer binding factor 2C expression in fetal mouse brain development. J Mol Neurosci 8:131–143.

Le Meur N, et al. (2010) MEF2C haploinsufficiency caused by either microdeletion of the 5q14.3 region or mutation is responsible for severe mental retardation with stereotypic movements, epilepsy and/or cerebral malformations. J Med Genet 47:22–29.

Liberman MC (2017) Noise-induced and age-related hearing loss: new perspectives and potential therapies. F1000Res 6:927.

Liberman MC, Kujawa SG (2017) Cochlear synaptopathy in acquired sensorineural hearing loss: manifestations and mechanisms. Hear Res 349:138–147.

Liu T, Li G, Noble KV, Li Y, Barth JL, Schulte BA, Lang H (2019) Age-dependent alterations of Kir4.1 expression in neural crest-derived cells of the mouse and human cochlea. Neurobiol Aging 80:210–222.

Lopez-Calderon J, Luck SJ (2014) ERPLAB: an open-source toolbox for the analysis of event-related potentials. Front Hum Neurosci 8:213.

Love MI, Huber W, Anders S (2014) Moderated estimation of fold change and dispersion for RNA-seq data with DESeq2. Genome Biol 15:550.

Lyons GE, Micales BK, Schwarz J, Martin JF, Olson EN (1995) Expression of mef2 genes in the mouse central nervous system suggests a role in neuronal maturation. J Neurosci 15:5727–5738.

Matsuka Y, Afroz S, Dalanon JC, Iwasa T, Waskitho A, Oshima M (2020) The role of chemical transmitters in neuron-glia interaction and pain in sensory ganglion. Neurosci Biobehav Rev 108:393–399.

McClaskey CM, Panganiban CH, Noble KV, Dias JW, Lang H, Harris KC (2020) A multi-metric approach to characterizing mouse peripheral auditory nerve function using the auditory brainstem response. J Neurosci Methods 346:108937.

McCullagh EA, Rotschafer SE, Auerbach BD, Klug A, Kaczmarek LK, Cramer KS, Kulesza RJ Jr, Razak KA, Lovelace JW, Lu Y, Koch U, Wang Y (2020) Mechanisms underlying auditory processing deficits in Fragile X syndrome. FASEB J 34:3501–3518.

Meyer W, Godynicki S, Tsukise A (2008) Lectin histochemistry of the endothelium of blood vessels in the mammalian integument, with remarks on the endothelial glycocalyx and blood vessel system nomenclature. Ann Anat 190:264–276.

Mikhail FM, et al. (2011) Clinically relevant single gene or intragenic deletions encompassing critical neurodevelopmental genes in patients with developmental delay, mental retardation, and/or autism spectrum disorders. Am J Med Genet 155:2386–2396.

Moreno-García A, Kun A, Calero O, Medina M, Calero M (2018) An overview of the role of lipofuscin in age-related neurodegeneration. Front Neurosci 12:464.

Naya FJ, Black BL, Wu H, Bassel-Duby R, Richardson JA, Hill JA, Olson EN (2002) Mitochondrial deficiency and cardiac sudden death in mice lacking the MEF2A transcription factor. Nat Med 8:1303–1309.

Pajevic S, Basser PJ, Fields RD (2014) Role of myelin plasticity in oscillations and synchrony of neuronal activity. Neuroscience 276:135–147.

Panganiban LH, Barth JL, Darbelli L, Xing Y, Zhang J, Li H, Noble KV, Liu T, Brown LN, Schulte BA, Richard S, Lang H (2018) Noise-induced dysregulation of Quaking RNA binding proteins contributes to auditory nerve demyelination and hearing loss. J Neurosci 38:2551–2568.

Panganiban CH, Barth JL, Tan J, Noble KV, McClaskey CM, Howard BA, Jafri SH, Dias JW, Harris KC, Lang H (2022) Two distinct types of nodes of Ranvier support auditory nerve function in the mouse cochlea. Glia 70:768–791.

Parthasarathy A, Bartlett EL, Kujawa SG (2019) Age-related changes in neural coding of envelope cues: peripheral declines and central compensation. Neuroscience 407:21–31.

Perkins G, Lee JH, Park S, Kang M, Perez-Flores MC, Ju S, Phillips G, Lysakowski A, Gratton MA, Yamoah EN (2020) Altered outer hair cell mitochondrial and subsurface cisternae connectomics are candidate mechanisms for hearing loss in mice. J Neurosci 40:8556–8572.

Petitpré C, Wu H, Sharma A, Tokarska A, Fontanet P, Wang Y, Helmbacher F, Yackle K, Silberberg G, Hadjab S, Lallemend F (2018) Neuronal heterogeneity and stereotyped connectivity in the auditory afferent system. Nat Commun 9:3691.

Pulipparacharuvil S, Renthal W, Hale CF, Taniguchi M, Xiao G, Kumar A, Russo SJ, Sikder D, Dewey CM, Davis MM, Greengard P, Nairn AC, Nestler EJ, Cowan CW (2008) Cocaine regulates MEF2 to control synaptic and behavioral plasticity. Neuron 59:621–633.

Riga D, Riga S, Halalau F, Schneider F (2006) Brain lipopigment accumulation in normal and pathological aging. Ann NY Acad Sci 1067:158–163.

Rocha H, Sampaio M, Rocha R, Fernandes S, Leão M (2016) MEF2C haploinsufficiency syndrome: report of a new MEF2C mutation and review. Eur J Med Genet 59:478–482.

Rojas D, Teale P, Maharajh K, Kronberg E, Youngpeter K, Wilson L, Wallace A, Hepburn S (2011) Transient and steady-state auditory gamma-band responses in first-degree relatives of people with autism spectrum disorder. Mol Autism 2:11.

Roper L, Arnold P, Monteiro B (2003) Co-occurrence of autism and deafness: diagnostic considerations. Autism 7:245–253.

Rosenhall U, Nordin V, Brantberg K, Gillberg C (2003) Autism and auditory brain stem responses. Ear Hear 24:206–214.

Rotschafer S, Razak K (2013) Altered auditory processing in a mouse model of fragile X syndrome. Brain Res 1506:12–24.

Rotschafer S, Cramer K (2017) Developmental emergence of phenotypes in the auditory brainstem nuclei of Fmr1 knockout mice. eNeuro 4: ENEURO.0264-17.2017.

Rotschafer SE, Marshak S, Cramer KS (2015) Deletion of Fmr1 alters function and synaptic inputs in the auditory brainstem. PLoS One 10: e0117266.

Salvi R, Sun W, Ding D, Chen G, Lobarinas E, Wang J, Radziwon K, Auerbach B (2017) Inner hair cell loss disrupts hearing and cochlear function leading to sensory deprivation and enhanced central auditory gain. Front Neurosci 10:621.

Santos M, Marques C, Nóbrega Pinto A, Fernandes R, Coutinho MB, Sousa CA (2017) Autism spectrum disorders and the amplitude of auditory brainstem response wave I. Autism Res 10:1300–1305.

Schrode KM, Muniak MA, Kim YH, Lauer AM (2018) Central compensation in auditory brainstem after damaging noise exposure. eNeuro 5: ENEURO.0250-18.2018.

Scott K, Schormans A, Pacoli K, De Oliveira C, Allman B, Schmid S (2018) Altered auditory processing, filtering, and reactivity in the cntnap2 Knock-out rat model for neurodevelopmental disorders. J Neurosci 38:8588–8604.

Sekerková G, Freeman D, Mugnaini E, Bartles JR (2005) Espin cytoskeletal proteins in the sensory cells of rodent taste buds. J Neurocytol 34:171–182.

Shi X (2011) Physiopathology of the cochlear microcirculation. Hear Res 282:10–24.

Speliotes EK, Kowall NW, Shanti BF, Kosofsky B, Finklestein SP, Leifer D (1996) Myocyte-specific enhancer binding factor 2C expression in gerbil brain following global cerebral ischemia. Neuroscience 70:67–77.

She H, Yang Q, Shepherd K, Smith Y, Miller G, Testa C, Mao Z (2011) Direct regulation of complex I by mitochondrial MEF2D is disrupted in a mouse model of Parkinson disease and in human patients. J Clin Invest 121:930–940.

Shrestha BR, Chia C, Wu L, Kujawa SG, Liberman MC, Goodrich LV (2018) Sensory neuron diversity in the inner ear is shaped by activity. Cell 174:1229–1246.

Smith A, Storti S, Lukose R, Kulesza R (2019) Structural and functional aberrations of the auditory brainstem in autism spectrum disorder. J Am Osteopath Assoc 119:41–50.

Song L, McGee J, Walsh EJ (2006) Frequency- and level-dependent changes in auditory brainstem responses (ABRS) in developing mice. J Acoust Soc Am 119:2242–2257.

Sulzer D, Mosharov E, Talloczy Z, Zucca FA, Simon JD, Zecca L (2008) Neuronal pigmented autophagic vacuoles: lipofuscin, neuromelanin, and ceroid as macroautophagic responses during aging and disease. J Neurochem 106:24–36.

Sun S, Babola T, Pregernig G, So KS, Nguyen M, Su SM, Palermo AT, Bergles DE, Burns JC, Müller U (2018) Hair cell mechanotransduction regulates spontaneous activity and spiral ganglion subtype specification in the auditory system. Cell 174:1247–1263.

Supek F, Bošnjak M, Škunca N, Šmuc T (2011) REVIGO summarizes and visualizes long lists of gene ontology terms. PLoS One 6:e21800.

Szymanski C, Brice P, Lam K, Hotto S (2012) Deaf children with autism spectrum disorders. J Autism Dev Disord 42:2027–2037.

Terman A, Gustafsson B, Brunk UT (2007) Autophagy, organelles and ageing. J Pathol 211:134–143.

Tonk V, Kyhm JH, Gibson CE, Wilson GN (2011) Interstitial deletion 5q14.3q21.3 with MEF2C haploinsufficiency and mild phenotype: when more is less. Am J Med Genet A 155A:1437–1441.

Tu S, et al. (2017) NitroSynapsin therapy for a mouse MEF2C haploinsufficiency model of human autism. Nat Commun 8:1488.

Velmeshev D, Schirmer L, Jung D, Haeussler M, Perez Y, Mayer S, Bhaduri A, Goyal N, Rowitch DH, Kriegstein AR (2019) Single-cell genomics identifies cell type-specific molecular changes in autism. Science 364:685–689.

Vila M (2019) Neuromelanin, aging, and neuronal vulnerability in Parkinson's disease. Mov Disord 34:1440–1451.

Voineagu I, Wang X, Johnston P, Lowe JK, Tian Y, Horvath S, Mill J, Cantor RM, Blencowe BJ, Geschwind DH (2011) Transcriptomic analysis of autistic brain reveals convergent molecular pathology. Nature 474:380–384.

Xing Y, Samuvel DJ, Stevens SM, Dubno JR, Schulte BA, Lang H (2012) Age-related changes in myelin basic protein in mouse and human auditory nerve. PLoS One 7:e34500.

Zhang W, Dai M, Fridberger A, Hassan A, Degagne J, Neng L, Zhang F, He W, Ren T, Trune D, Auer M, Shi X (2012) Perivascular-resident macrophage-like melanocytes in the inner ear are essential for the integrity of the intrastrial fluid-blood barrier. Proc Natl Acad Sci USA 109:10388–10393.

Zweier M, Gregor A, Zweier C, Engels H, Sticht H, Wohlleber E, Bijlsma EK, Holder SE, Zenker M, Rossier E, Grasshoff U, Johnson DS, Robertson L, Firth HV, Kraus C, Ekici AB, Reis A, Rauch A (2010) Mutations in MEF2C from the 5q14.3q15 microdeletion syndrome region are a frequent cause of severe mental retardation and diminish MECP2 and CDKL5 expression. Hum Mutat 31:722–733.